INTERNATIONAL ATOMIC ENERGY AGENCY
UNITED NATIONS EDUCATIONAL, SCIENTIFIC AND CULTURAL ORGANIZATION

INTERNATIONAL CENTRE FOR THEORETICAL PHYSICS
34100 TRIESTE (ITALY) - P.O.B. 586 - MIRAMARE - STRADA COSTIERA 11 - TELEPHONE: 2240-1
CABLE: CENTRATOM - TELEX 460392-1

H4.SMR/303 -12

WORKSHOP
GLOBAL GEOPHYSICAL INFORMATICS WITH APPLICATIONS TO RESEARCH IN EARTHQUAKE PREDICTIONS AND REDUCTION OF SEISMIC RISK

(15 November - 16 December 1988)

CONSTRUCTION OF SYNTHETIC SEISMOGRAMS

G. PANZA

Università degli Studi di Trieste
Istituto di Geodesia e Geofisica
Via Dell'Universita 7
34123 Trieste

CONTENTS

INTERNATIONAL CENTRE FOR THEORETICAL PHYSICS

Miramare - Trieste, Italy

WORKSHOP

GLOBAL GEOPHYSICAL INFORMATICS WITH APPLICATIONS TO RESEARCH IN EARTHQUAKE PREDICTIONS AND REDUCTION OF SEISMIC RISK

(15 November - 16 December 1988)

CONSTRUCTION OF SYNTHETIC SEISMOGRAMS

by

G. F. Panza

Institute of Geodesy and Geophysics, University of Trieste

International School for Advanced Studies, Trieste

1. Introduction

Currently the interest of seismologists and theoreticians focuses strongly on methods which allow the treatment of laterally heterogeneous media. This development has been prompted by many clear perceptions, collected in several disciplines of geosciences, that the earth is a dynamic body with relatively rapid internal motions. These processes and related horizontal temperature differences may lead to pronounced lateral variations in elastic and anelastic properties. Thus, for the seismologist, who is interested in depth ranges from the lower crust to the core,

the earth becomes what it has always been for those engaged in seismic prospecting: a medium with truly three-dimensional inhomogeneities.

Methods for horizontally stratified earth models will, however, continue to have their importance and find applications in studies of structural properties and sources of seismic waves. Hence, a good understanding of the relevant theory will always be a necessity and not only as a premise for the treatment of lateral variations. The purpose of these lecture notes is to contribute to this understanding by presenting a self-contained theory of one of the methods for horizontally layered media, the modal summation method, including all material that is necessary for the development of corresponding computer programs for theoretical seismograms.

Before we start with the details, a few words about the general scene of methods for horizontally stratified media are in order. This scene is very vast now, and it is practically impossible to mention all the different methods that are in use. Much background material can be found in the text books and monographs by Pilant (1979), Aki and Richards (1980), Ben-Menahem and Singh (1981) and Kennett (1983). The most important theories and methods for wave propagation and seismogram synthesis are the following (the references given are only examples and far from complete):

Generalized ray theory (Helmberger, 1968; Müller, 1969; Ben-Menahem and Vered, 1973): the medium is approximated by homogeneous layers, and the wave field is decomposed into elementary seismograms corresponding to rays.

Full-wave theory (Cormier and Richards, 1977): a ray theory for inhomogeneous layers which takes account of frequency-dependent effects connected, e.g., with caustics and shadow zones.

WKBJ theory (Chapman, 1978): a ray theory for inhomogeneous layers which is more limited than full-wave theory, as far as frequency-dependent effects are concerned, but which allows very rapid computations.

Wavenumber or slowness integration methods (Fuchs, 1968; Fuchs and Müller, 1971; Kind, 1978; Cormier, 1980; Wang and Herrmann, 1980; Ingate et al., 1983; Ha, 1984): representation of the Fourier-transformed wave field of a layered medium by integrals over horizontal wavenumber or slowness.

Wavenumber summation methods (Alekseev and Mikhailenko, 1980; Bouchon, 1981; Korn and Müller, 1983; Spudich and Ascher, 1983; Olson et al., 1984; Campillo et al., 1984): both time- and frequency-domain methods which are in principle very similar to wavenumber integration methods, but the continuous distribution of wavenumbers is replaced by a discrete one.

Modal summation method (Harvey, 1981; Panza, 1985): representation of the wave field by normal modes of Rayleigh and Love waves alone, either with the assumption of a perfect reflector at depth or without.

The first three of these methods are suitable for the calculation of body-wave contributions to seismograms, whereas the last three also allow surface waves to be included, i.e. these methods are methods for complete seismograms.

The modal summation methods has its roots in Pekeris (1948) pioneering work. In fact he has shown the possibility of treating the problem of wave propagation in homogeneous layered media, both in terms of rays (ray-theory) and in terms of modes (normal mode solution); he also proposed the use of ray theory for the purpose of determining the beginning of the record at a distant point or for determining the steady-state solution up to moderate ranges. On the other hand, if one is interested in the steady-state solution at large ranges where many rays need to be considered, or in the later phases received at large distances, the normal mode solution is preferable.

A great concentration of effort to understand the way in which the features of observed seismograms are related to the properties of the source and structure of the Earth is based on a variety of mathematical and physical

tools essentially inspired by the ray-theory and its developments.

Quite recently, as a natural consequence of the explicit statement of the details of high-frequency eigenvalue and eigenfunctions evaluation, large-scale application of multimode synthetic seismograms, for frequencies as high as 10 Hz, has received the due consideration (Panza, 1985; Suhadolc and Panza, 1985; Chiaruttini, Costa and Panza, 1985; Panza, Suhadolc and Chiaruttini, 1986; Panza and Suhadolc, 1986).

These lecture notes are organized as follows. After a brief discussion, in Section 2, of the differential equations for wave propagation in horizontally stratified media and of the boundary conditions proper for surface waves we describe in Section 3 the essential features of the fast version (Schwab, 1970) of Knopoff's matrix method (Knopoff, 1964a) for elastic wave problems, while in Section 4 we discuss the main ideas about eigenfunctions computations (Schwab et al., 1984). In Section 5 we describe in detail some practical computational aspects: the mode follower and the structure minimization (Panza and Suhadolc, 1986). In Section 6 we give some details about the computations of the main effects of anelasticity. In Section 7 we discuss the response to buried sources. In the final Section we give examples of the computation of synthetic

signals and their comparison with real data. All the material above will be described for P-SV type of motion (Rayleigh waves), however all the main results and ideas are valid also for SH type of motion (Love waves).

2. Differential equations and boundary conditions

We assume that the medium consists of homogeneous layers, separated by first-order discontinuities. If a medium is continuously inhomogeneous (throughout or piecewise), it is replaced by a sufficiently large number of homogeneous layers; in smooth gradient zones it is usually enough to choose roughly half the dominant wavelength as layer thickness, whereas in transition zones with larger velocity gradients the layer thickness should be reduced further. The advantage of the homogeneous-layer approximation is that inside each layer the equation of motion takes a relatively simple form. Its disadvantage is that boundary conditions have to be fulfilled at many interfaces. Analytical methods for inhomogeneous layers (in contrast to numerical, e.g. finite-difference, methods) are not yet developed to a point where they really can compete with the methods for homogeneous layers.

The equation of motion of a homogeneous, isotropic elastic medium is

$$\rho\ddot{\mathbf{u}} = (\lambda+2\mu)\,\mathrm{grad\ div}\ \mathbf{u} - \mu\ \mathrm{rot\ rot}\ \mathbf{u}, \qquad (1)$$

where $\mathbf{u}$ is the displacement vector, ρ the density and λ and μ the Lamé parameters. Body forces due to gravity and seismic sources are not included in Eq. (1): it is assumed that gravity has no other effect than to determine, via self-compression, the (constant) values of ρ, λ and μ, and sources of seismic waves are included through their known contributions to $\mathbf{u}$ (e.g. Harkrider, 1970) (see Section 7).

In order to simplify the discussion as far as possible, we shall consider solutions of the elastic equations of motion in the form of plane waves rather than attempt to treat the more complex case of waves diverging from a point-source. This does not involve loss of generality in the computation of the dispersion function since the point-source solution may be developed by integration of plane-wave solutions (e.g. Harkrider, 1964).

Let us consider plane waves of angular frequency p and horizontal phase velocity c propagated in a semi-infinite medium made up of n parallel, homogeneous, isotropic layers. In these lectures, all layers will be assumed to be solid; the case of a fluid layer can be easily found in the referenced literature. The x axis is taken parallel to the layers with the positive sense in the

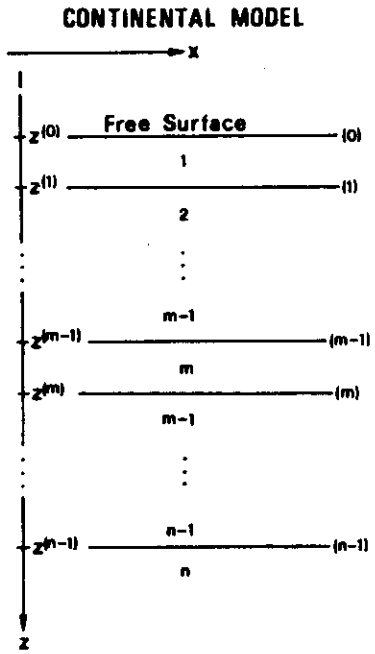

Fig. 1. Direction of axes and numbering of layers and interfaces.

direction of propagation. The positive z axis is taken as directed into the medium. The various layers and interfaces are numbered away from the free surface, as shown in figure 1. We confine our attention to waves of Rayleigh type (P-SV motion), by which we mean that there is no displacement in the y direction and that the amplitude diminishes exponentially in the +z direction in the semi-infinite layer.

For the m-th layer let

ρ_m = density, d_m = thickness, λ_m, μ_m = Lamé elastic constants,

$\alpha_m = \left[(\lambda_m+2\mu_m)/\rho_m\right]^{\frac{1}{2}}$ = velocity of propagation of dilatational waves

$\beta_m = \left[\mu_m/\rho_m\right]^{\frac{1}{2}}$ = velocity of propagation of rotational waves

$k = p/c = 2\pi$/wave length (horizontal)

$$r_{\alpha_m} = \begin{cases} +\left[(c/\alpha_m)^2-1\right]^{\frac{1}{2}} & \text{if } c>\alpha_m \\ -i\left[1-(c/\alpha_m)^2\right]^{\frac{1}{2}} & \text{if } c<\alpha_m \end{cases} \qquad \text{if } m<n$$

$$r_{\beta_m} = \begin{cases} +\left[(c/\beta_m)^2-1\right]^{\frac{1}{2}} & \text{if } c>\beta_m \\ -i\left[1-(c/\beta_m)^2\right]^{\frac{1}{2}} & \text{if } c<\beta_m \end{cases}$$

$$r_{\alpha_m} = -i(1-c^2/\alpha_m^2)^{\frac{1}{2}} \qquad \text{if } m=n$$

$r_{\beta_m} = -i(1-c^2/\beta_m^2)^{\frac{1}{2}}$

$\gamma_m = 2(\beta_m/c)^2$

u_m, w_m = displacement components in x and z directions

σ_m = normal stress

τ_m = tangential stress

Then, as is well known, periodic solutions of the elastic equation of motion for the m-th layer may be found by combining dilatational wave solutions,

$$\Delta_m=(\partial u_m/\partial x)+(\partial w_m/\partial z)= \tag{2}$$

$$=\exp[i(pt-kx)][\Delta'_m\exp(-ikr_{\alpha_m}z)+\Delta''_m\exp(ikr_{\alpha_m}z)$$

with rotational wave solutions,

$$\omega_m=(1/2)[(\partial u_m/\partial z)-(\partial w_m/\partial x)]= \tag{3}$$

$$=\exp[i(pt-kx)][\omega'_m\exp(-ikr_{\beta_m}z)+\omega''_m\exp(ikr_{\beta_m}z)$$

where Δ'_m, Δ''_m, ω'_m and ω''_m are constants. With the sign conventions defined above, the term in Δ'_m represents a plane wave whose direction of propagation makes an angle $\cot^{-1} r_{\alpha_m}$ with the +z direction when r_{α_m} is real, and a wave propagated in the +x direction with amplitude diminishing exponentially in the +z direction when r_{α_m} is imaginary. Similarly, the term in Δ''_m represents a plane wave making the same angle with the -z direction when r_{α_m} is real and a wave propagated in the +x direction with amplitude increasing exponentially in the +z direction when r_{α_m} is imaginary. The same remarks apply to the terms in ω'_m and

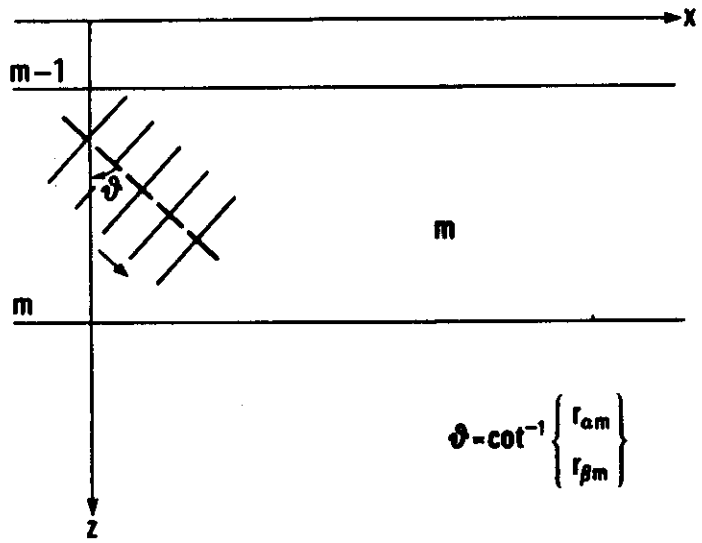

Fig. 2a. Plane waves associated to Δ'_m or ω'_m when r_{α_m} (P-wave) or r_{β_m} (S-wave) are real.

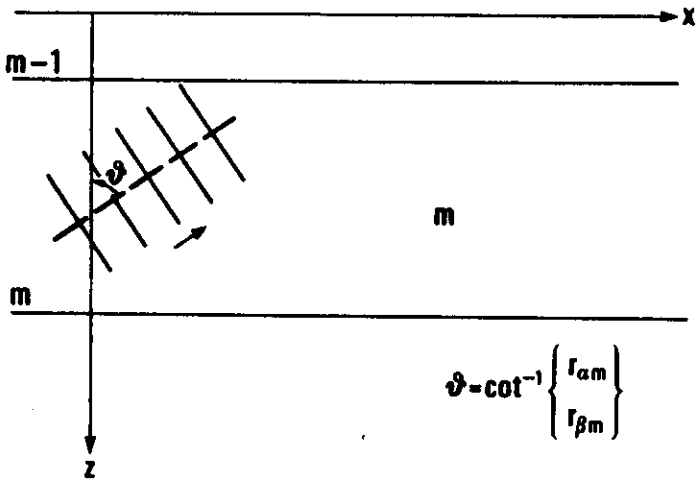

Fig. 2b. Plane waves associated to Δ''_m or ω''_m when r_{α_m} (P-wave) or r_{β_m} (S-wave) are real.

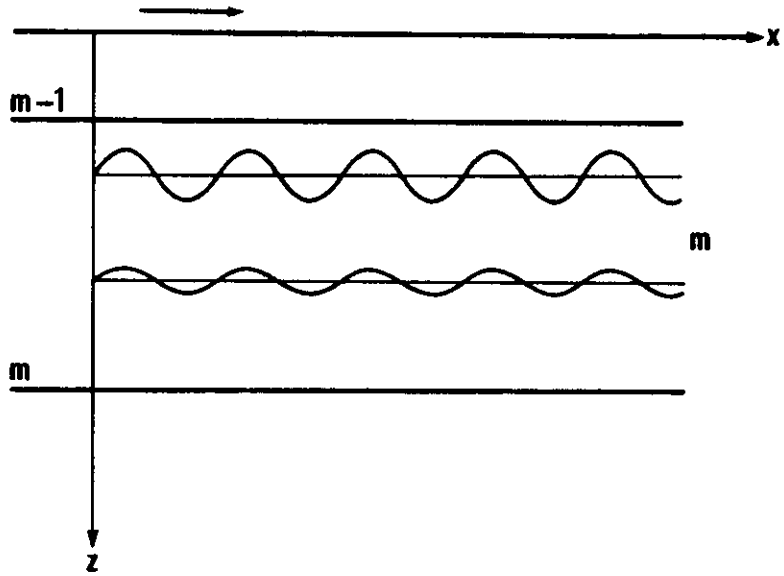

Fig. 2c. Wave propagating in the x direction with amplitude decreasing with increasing depth associated to Δ'_m or ω'_m when r_{α_m} (P-wave) or r_{β_m} (S-wave) are imaginary.

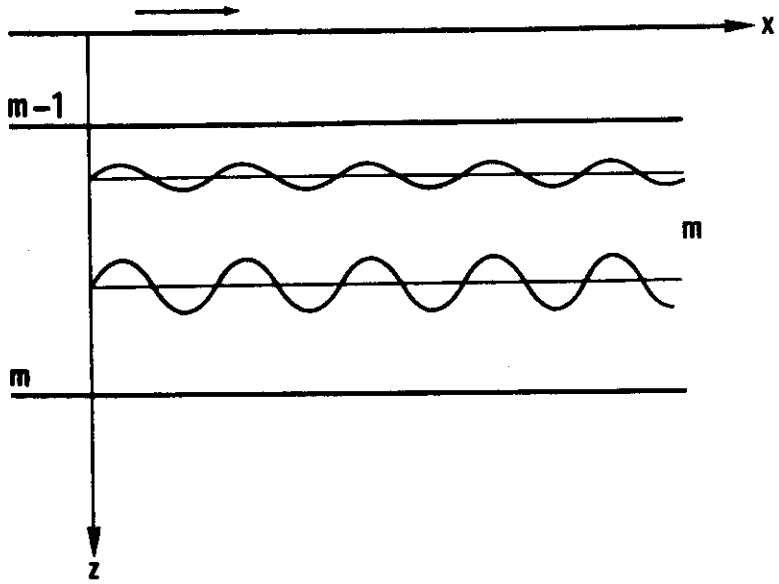

Fig. 2d. Wave propagating in the x direction with amplitude increasing with increasing depth associated to Δ_m'' or ω_m'' when r_{α_m} (P-wave) or r_{β_m} (S-wave) are imaginary.

ω_m'' with r_{β_m} substituted for r_{α_m} (see Fig. 2a, 2b, 2c, 2d).

The displacements and the pertinent stress components corresponding to the dilatation and rotation given by (2) and (3) are,

$$u_m=-(\alpha_m/p)^2(\partial\Delta_m/\partial x)-2(\beta_m/p)^2(\partial\omega_m/\partial z) \tag{4}$$

$$w_m=-(\alpha_m/p)^2(\partial\Delta_m/\partial z)+2(\beta_m/p)^2(\partial\omega_m/\partial x) \tag{5}$$

$$\sigma_m=\rho_m[\alpha_m^2\Delta_m+2\beta_m^2\{(\alpha_m/p)^2(\partial^2\Delta_m/\partial x^2)+ +2(\beta_m/p)^2(\partial^2\omega_m/\partial x\partial z)\}] \tag{6}$$

$$\tau_m=2\rho_m\beta_m^2[-(\alpha_m/p)^2(\partial^2\Delta_m/\partial x\partial z)+ +(\beta_m/p)^2\{(\partial^2\omega_m/\partial x^2)-(\partial^2\omega_m/\partial z^2)\}] \tag{7}$$

The boundary conditions to be met at an interface between two layers require that these four quantities should be continuous. Continuity of the displacements is assured if the corresponding velocity components $\dot{u}_m$ and $\dot{w}_m$ are made continuous and, since c is the same in all layers, we may take the dimensionless quantities $\dot{u}_m/c$ and $\dot{w}_m/c$ to be continuous. Substituting the expressions (2) and (3) in

equations (4) to (7) and expressing the exponental functions of ikrz in trigonometric form, we find

$$
\begin{aligned}
c\,u_m &= A_m \cos p_m - i B_m \sin p_m \\
&\quad + r_{\beta_m} C_m \cos q_m - i r_{\beta_m} D_m \sin q_m, \\
c\,w_m &= -i r_{\alpha_m} A_m \sin p_m + r_{\alpha_m} B_m \cos p_m \\
&\quad + i C_m \sin q_m - D_m \cos q_m, \\
\sigma_m &= \rho_m(\gamma_m - 1) A_m \cos p_m - i \rho_m(\gamma_m - 1) \\
&\quad \cdot B_m \sin p_m + \rho_m \gamma_m r_{\beta_m} C_m \cos q_m \\
&\quad - i \rho_m \gamma_m r_{\beta_m} D_m \sin q_m, \\
\tau_m &= i \rho_m \gamma_m r_{\alpha_m} A_m \sin p_m - \rho_m \gamma_m r_{\alpha_m} \\
&\quad \cdot B_m \cos p_m - i \rho_m(\gamma_m - 1) C_m \sin q_m \\
&\quad + \rho_m(\gamma_m - 1) D_m \cos q_m,
\end{aligned}
\tag{8}
$$

where

$$
\begin{aligned}
A_m &= -\alpha_m^2(\Delta'_m + \Delta''_m), \qquad B_m = -\alpha_m^2(\Delta'_m - \Delta''_m), \\
C_m &= -2\beta_m^2(\omega'_m - \omega''_m), \quad D_m = -2\beta_m^2(\omega'_m + \omega''_m), \\
p_m &= k r_{\alpha_m}[z - z^{(m-1)}], \quad q_m = k r_{\beta_m}[z - z^{(m-1)}],
\end{aligned}
\tag{9}
$$

ρ_m is the density, $z^{(m-1)}$ is the depth of the upper interface of the m-th layer and Δ'_m, Δ''_m, ω'_m, ω''_m are Haskell (1953) constants appearing in the depth-dependent part of the dilatational and rotational wave solutions:

$$
\begin{aligned}
&\Delta'_m \exp(-ik r_{\alpha_m} z) + \Delta''_m \exp(ik r_{\alpha_m} z), \\
&\omega'_m \exp(-ik r_{\beta_m} z) + \omega''_m \exp(ik r_{\beta_m} z).
\end{aligned}
\tag{10}
$$

3. Fast version of Knopoff's method

For a continental model, the vanishing of the two components of stress at the free surface yields:

$$
\begin{aligned}
-\rho_1(\gamma_1 - 1) A_1 - \rho_1 \gamma_1 r_{\beta_1} C_1 &= 0, \\
\rho_1 \gamma_1 r_{\alpha_1} B_1 - \rho_1(\gamma_1 - 1) D_1 &= 0.
\end{aligned}
\tag{11}
$$

Thus Knopoff's submatrix $A^{(0)}$ can be written in the form

$$
A^{(0)} = \begin{bmatrix} -\rho_1(\gamma_1 - 1) & 0 & -\rho_1 \gamma_1 & 0 \\ 0 & \rho_1 \gamma_1 & 0 & -\rho_1(\gamma_1 - 1) \end{bmatrix}. \tag{12}
$$

At the m-th interface, the continuity of displacement and stress yields

$$
\begin{aligned}
&A_m\cos P_m - iB_m\sin P_m + r_{\beta_m}C_m\cos Q_m - ir_{\beta_m}D_m\sin Q_m \\
&\quad = A_{m+1} + r_{\beta_{m+1}}C_{m+1}, \\
&-ir_{\alpha_m}A_m\sin P_m + r_{\alpha_m}B_m\cos P_m + iC_m\sin Q_m - D_m\cos Q_m \\
&\quad = r_{\alpha_{m+1}}B_{m+1} - D_{m+1}, \\
&\rho_m(\gamma_m-1)A_m\cos P_m - i\rho_m(\gamma_m-1)B_m\sin P_m \\
&\qquad + \rho_m\gamma_m r_{\beta_m}C_m\cos Q_m - i\rho_m\gamma_m r_{\beta_m}D_m\sin Q_m \\
&\quad = \rho_{m+1}(\gamma_{m+1}-1)A_{m+1} + \rho_{m+1}\gamma_{m+1}r_{\beta_{m+1}}C_{m+1}, \\
&i\rho_m\gamma_m r_{\alpha_m}A_m\sin P_m - \rho_m\gamma_m r_{\alpha_m}B_m\cos P_m \\
&\qquad - i\rho_m(\gamma_m-1)C_m\sin Q_m + \rho_m(\gamma_m-1)D_m\cos Q_m \\
&\quad = -\rho_{m+1}\gamma_{m+1}r_{\alpha_{m+1}}B_{m+1} + \rho_{m+1}(\gamma_{m+1}-1)D_{m+1},
\end{aligned}
\tag{13}
$$

where $P_m = kr_{\alpha_m}d_m$, $Q_m = kr_{\beta_m}d_m$ and d_m is the layer thickness. Thus, Knopoff's 4x8 interface submatrices have the form

$$
\Lambda^{(m)} = \begin{bmatrix}
\cos P_m & -i\sin P_m/r_{\alpha_m} & \cos Q_m & \\
-ir_{\alpha_m}\sin P_m & \cos P_m & i\sin Q_m/r_{\beta_m} & \\
\rho_m(\gamma_m-1)\cos P_m & -i\rho_m(\gamma_m-1)\sin P_m/r_{\alpha_m} & \rho_m\gamma_m\cos Q_m & \\
i\rho_m\gamma_m r_{\alpha_m}\sin P_m & -\rho_m\gamma_m\cos P_m & -i\rho_m(\gamma_m-1)\sin Q_m/r_{\beta_m} & \\
-ir_{\beta_m}\sin Q_m & -1 & 0 & -1 & 0 \\
-\cos Q_m & 0 & -1 & 0 & 1 \\
-i\rho_m\gamma_m r_{\beta_m}\sin Q_m & -\rho_{m+1}(\gamma_{m+1}-1) & 0 & -\rho_{m+1}\gamma_{m+1} & 0 \\
\rho_m(\gamma_m-1)\cos Q_m & 0 & \rho_{m+1}\gamma_{m+1} & 0 & -\rho_{m+1}(\gamma_{m+1}-1)
\end{bmatrix}
\tag{14}
$$

and, noting that in the half-space $A_n = B_n = -\alpha^2_n\,\Delta'_n$

$C_n = D_n = -2\beta^2_n\,\omega'_n$, the submatrix representing the (n-1)th interface has the form

$$
\Lambda^{(n-1)} = \begin{bmatrix}
\cdots & -1 & -r_{\beta_n} \\
\cdots & -r_{\alpha_n} & 1 \\
\cdots & -\rho_n(\gamma_n-1) & -\rho_n\gamma_n r_{\beta_n} \\
\cdots & \rho_n\gamma_n r_{\alpha_n} & -\rho_n(\gamma_n-1)
\end{bmatrix},
\tag{15}
$$

where the first four columns are the same as those of $\Lambda^{(m)}$ with m=n-1. It may be worth observing here that, for each layer, $\Lambda^{(i)}$ (i=1,n) submatrices represent the denominators of Cramer's system solutions when the boundary conditions are applied.

In more compact notation we can write

$$
\Delta_n = \begin{vmatrix}
\Lambda^{(0)} & & & \\
\Lambda^{(1)} & & & \\
 & \ddots & & \\
 & & \Lambda^{(n-2)} & \\
 & & & \Lambda^{(n-1)}
\end{vmatrix}
\tag{16}
$$

where the non-zero elements only are pictured.

A condition for surface waves to exist is $\Delta_R=0$, which defines the dispersion function for Rayleigh waves

$$F_R(p,c) = \Delta_R = 0 \tag{17}$$

If we limit our attention to the case of solid Earth models, the Rayleigh wave dispersion function, $F_R(p,c)$, has the form

$$F_R(p,c)=T^{(o)}\overline{F}^{(1)}F^{(2)}\overline{F}^{(3)}\cdots \begin{cases} F^{(n-2)}\overline{F}^{(n-1)}T^{(n)}_{solid} & \text{(a)} \\ \overline{F}^{(n-2)}F^{(n-1)}\overline{T}^{(n)}_{solid} & \text{(b)} \end{cases} \tag{18}$$

(a) if n is even,

(b) if n is odd.

which has the symbolic matrix form (1x6)(6x6)...(6x6)(6x1). The elements of these matrices are

$$T^{(o)} = [-\gamma_1(\gamma_1-1), 0, (\gamma_1-1)^2, \gamma_1^2, \quad 0 \quad , \gamma_1(\gamma_1-1)]. \tag{19}$$

$$F^{(m)} = \begin{bmatrix} F^{(m)}_{1212} & F^{(m)}_{1213} & F^{(m)}_{1214} & F^{(m)}_{1223} & F^{(m)}_{1224} & F^{(m)}_{1234} \\ F_{1312} & F_{1313} & F_{1314} & F_{1323} & F_{1324} & F_{1334} \\ F_{1412} & F_{1413} & F_{1414} & F_{1423} & F_{1424} & F_{1434} \\ F_{2312} & F_{2313} & F_{2314} & F_{2323} & F_{2324} & F_{2334} \\ F_{2412} & F_{2413} & F_{2414} & F_{2423} & F_{2424} & F_{2434} \\ F_{3412} & F_{3413} & F_{3414} & F_{3423} & F_{3424} & F_{3434} \end{bmatrix}, \tag{20}$$

$$F^{(m)} = \begin{bmatrix} F^{(m)}_{3434} & -F^{(m)}_{3424} & F^{(m)}_{3423} & F^{(m)}_{3414} & -F^{(m)}_{3413} & F^{(m)}_{3412} \\ -F_{2434} & F_{2424} & -F_{2423} & -F_{2414} & F_{2413} & -F_{2412} \\ F_{2334} & -F_{2324} & F_{2323} & F_{2314} & -F_{2313} & F_{2312} \\ F_{1434} & -F_{1424} & F_{1423} & F_{1414} & -F_{1413} & F_{1412} \\ -F_{1334} & F_{1324} & -F_{1323} & -F_{1314} & F_{1313} & -F_{1312} \\ F_{1234} & -F_{1224} & F_{1223} & F_{1214} & -F_{1213} & F_{1212} \end{bmatrix}, \tag{21}$$

$$T^{(n)}_{solid} = \begin{bmatrix} 0 \\ -r_{\alpha\alpha} \\ r_{\alpha\alpha}r_{\beta\alpha} \\ 1 \\ -r_{\beta\alpha} \\ 0 \end{bmatrix}\varepsilon, \qquad \overline{T}^{(n)}_{solid} = \begin{bmatrix} 0 \\ r_{\beta\alpha} \\ 1 \\ r_{\alpha\alpha}r_{\beta\alpha} \\ r_{\alpha\alpha} \\ 0 \end{bmatrix}\varepsilon, \tag{22}$$

The elements $F^{(m)}_{ijkl}$ are obtained from Table I. The quantity $\varepsilon=(-1)^{n-1}\rho^2_1 c^2/\gamma_n r_{\alpha n} r_{\beta n}\rho^2_n\alpha^2_n$ is included in (22) in order that F_R have the same numerical value as the dispersion functions from the Δ-matrix extensions, and the product form of the original Thomson-Haskell formulation.

The basic interface-matrix multiplication in (18) has the symbolic matrix form (1x6)(6x6), where the sixth element of the 1x6 matrix is always the negative of the first element. The symmetry of the 6x6 interface matrices, as indicated below,

$$[U^{(m+1)}, iV^{(m+1)}, W^{(m+1)}, R^{(m+1)}, iS^{(m+1)}, -U^{(m+1)}]$$

$$=[U^{(m)}, iV^{(m)}, W^{(m)}, R^{(m)}, iS^{(m)}, -U^{(m)}]\begin{bmatrix}\delta & 0 & \nu & \upsilon & 0 & \eta\\ i\kappa & \cdot & \cdot & \cdot & \cdot & -i\kappa\\ \theta & \cdot & \cdot & \cdot & \cdot & -\theta\\ \phi & \cdot & \cdot & \cdot & \cdot & -\phi\\ i\iota & \cdot & \cdot & \cdot & \cdot & -i\iota\\ \eta & 0 & -\nu & -\upsilon & 0 & \delta\end{bmatrix} \quad (23)$$

is the reason that the 1x6 matrix retains this property throughout the formation of the interface-matrix product. The first and last elements of columns 2 and 5 of the 6x6 matrix vanish, which means that fourth-, not sixth-order matrix multiplication is involved in forming the corresponding elements of the 1x6 product matrix. The remaining four elements of the product matrix involve only fifth-order multiplication due to the properties of the

TABLE I

EXPRESSIONS FOR THE QUANTITIES F_{ijkl}

kl / ij	12	13	14	23	24	34
12	$-\varepsilon^{(m)}_6$	0	$\varepsilon^{(m)}_{13}$	$\varepsilon^{(m)}_8$	0	$\varepsilon^{(m)}_{10}$
13	$-H(\varepsilon_{11}\zeta_9+\varepsilon_7\zeta_{10})$	$\varepsilon_{15}\zeta_{10}$	$H(\varepsilon_{14}\zeta_9+\varepsilon_{13}\zeta_{10})$	$H(\varepsilon_9\zeta_9+\varepsilon_5\zeta_{10})$	$-\varepsilon_{15}\zeta_7$	$H(\varepsilon_{11}\zeta_9+\varepsilon_7\zeta_{10})$
14	$\varepsilon_{11}\zeta_7-\varepsilon_7\zeta_{12}$	$H(\varepsilon_{15}\zeta_{10})$	$-\varepsilon_{14}\zeta_7+\varepsilon_{13}\zeta_{12}$	$-\varepsilon_9\zeta_7+\varepsilon_5\zeta_{12}$	$H(\varepsilon_{15}\zeta_9)$	$-\varepsilon_{11}\zeta_7+\varepsilon_7\zeta_{12}$
23	$-\varepsilon_{15}\zeta_{12}+\varepsilon_7\zeta_7$	$H(\varepsilon_{15}\zeta_9)$	$\varepsilon_{14}\zeta_{12}-\varepsilon_{13}\zeta_7$	$\varepsilon_9\zeta_{12}-\varepsilon_5\zeta_7$	$H(\varepsilon_{15}\zeta_{11})$	$\varepsilon_{15}\zeta_{12}-\varepsilon_7\zeta_7$
24	$-H(\varepsilon_{11}\zeta_{11}+\varepsilon_7\zeta_9)$	$-\varepsilon_{15}\zeta_7$	$H(\varepsilon_{14}\zeta_{11}+\varepsilon_{13}\zeta_9)$	$H(\varepsilon_9\zeta_{11}+\varepsilon_5\zeta_9)$	$\varepsilon_{15}\zeta_{12}$	$H(\varepsilon_{11}\zeta_{11}+\varepsilon_7\zeta_9)$
34	ε_{10}	0	$-\varepsilon_{15}$	$-\varepsilon_9$	0	$-\varepsilon_8$

$\varepsilon^{(m)}_0=\rho_{m+1}/\rho_m$ $\quad \varepsilon^{(m)}_1=\varepsilon^{(m)}_4\varepsilon^{(m)}_6$ $\quad \zeta^{(m)}_1=\cos P_m$ $\quad \zeta^{(m)}_7=\zeta^{(m)}_1\zeta^{(m)}_6$

$\varepsilon_1=\gamma_m-\varepsilon_0\gamma_{m+1}$ $\quad \varepsilon_6=\varepsilon^2_3$ $\quad \zeta_2=\cos Q_m$ $\quad \zeta_8=\zeta_1\zeta_2$

$\varepsilon_2=\varepsilon_1-1$ $\quad \varepsilon_{10}=\varepsilon_3\varepsilon_5$ $\quad \zeta_3=r_m\sin P_m$ $\quad \zeta_9=\zeta_1\zeta_3$

$\varepsilon_3=\varepsilon_1+\varepsilon_0$ $\quad \varepsilon_{11}=\varepsilon_3\varepsilon_4$ $\quad \zeta_4=\sin P_m/r_m$ $\quad \zeta_{10}=\zeta_3\zeta_4$

$\varepsilon_4=\varepsilon_2+\varepsilon_0$ $\quad \varepsilon_{12}=\varepsilon^2_3$ $\quad \zeta_5=r_m\sin Q_m$ $\quad \zeta_{11}=\zeta_4\zeta_5$

$\varepsilon_5=\varepsilon^2_1$ $\quad \varepsilon_{13}=\varepsilon_3\varepsilon_4$ $\quad \zeta_6=\sin Q_m/r_m$ $\quad \zeta_{12}=\zeta_5\zeta_6$

$\varepsilon_6=\varepsilon_1\varepsilon_2$ $\quad \varepsilon_{14}=\varepsilon^2_4$ $\quad \zeta_7=\zeta_1\zeta_6$ $\quad \zeta_{13}=\zeta_4\zeta_6$

$\varepsilon_7=\varepsilon_1\varepsilon_3$ $\quad \varepsilon_{15}=-\varepsilon_0$ $\quad \zeta_8=\zeta_1\zeta_5$

$\varepsilon_{16}=\varepsilon_0+\varepsilon_{10}$

first and last elements of the 1x6 matrices. Since the first and last elements of the product matrix are the same except for sign, only one of these two elements needs to be computed. Two fourth-order and three fifth-order multiplications per matrix product is a significant improvement over the original six sixth-order multiplications. If these five product-matrix elements are written out analytically, it is seen that there is still considerable simplification possible by means of simple algebraic factorization. The results of this factorization allow the elements of the product matrix to be written in very simple form. Combining the results of this factorization with the formation of the elements of the new, (m+1)th, 6x6 matrix produces the key portion of the "fast" form of Knopoff's method for Rayleigh wave dispersion computations: For m+1 even,

$$
\begin{aligned}
U^{(m+1)} &= -\varepsilon_{16}^{(m+1)}U^{(m)} + \varepsilon_{11}^{(m+1)}K^{(m+1)} + \varepsilon_{7}^{(m+1)}L^{(m+1)},\\
V^{(m+1)} &= \varepsilon_{13}^{(m+1)}(\zeta_{14}^{(m+1)}V^{(m)} + \zeta_{10}^{(m+1)}W^{(m)} + \zeta_{9}^{(m+1)}R^{(m)} - \zeta_{7}^{(m+1)}S^{(m)}),\\
W^{(m+1)} &= -\varepsilon_{14}^{(m+1)}K^{(m+1)} - \varepsilon_{12}^{(m+1)}L^{(m+1)} + 2\varepsilon_{13}^{(m+1)}U^{(m)},\\
R^{(m+1)} &= -\varepsilon_{9}^{(m+1)}K^{(m+1)} - \varepsilon_{5}^{(m+1)}L^{(m+1)} + 2\varepsilon_{6}^{(m+1)}U^{(m)},\\
S^{(m+1)} &= \varepsilon_{13}^{(m+1)}(-\zeta_{7}^{(m+1)}V^{(m)} + \zeta_{8}^{(m+1)}W^{(m)} + \zeta_{11}^{(m+1)}R^{(m)} + \zeta_{13}^{(m+1)}S^{(m)}),
\end{aligned}
\tag{24}
$$

where

$$
\begin{aligned}
K^{(m+1)} &= \zeta_{9}^{(m+1)}V^{(m)} + \zeta_{7}^{(m+1)}W^{(m)} - \zeta_{15}^{(m+1)}R^{(m)} + \zeta_{11}^{(m+1)}S^{(m)},\\
L^{(m+1)} &= \zeta_{10}^{(m+1)}V^{(m)} - \zeta_{12}^{(m+1)}W^{(m)} + \zeta_{7}^{(m+1)}R^{(m)} + \zeta_{8}^{(m+1)}S^{(m)},
\end{aligned}
\tag{25}
$$

and for m+1 odd,

$$
\begin{aligned}
U^{(m+1)} &= -\varepsilon_{16}^{(m+1)}U^{(m)} + \varepsilon_{11}^{(m+1)}X^{(m+1)} + \varepsilon_{7}^{(m+1)}Z^{(m+1)},\\
V^{(m+1)} &= \varepsilon_{13}^{(m+1)}(\zeta_{13}^{(m+1)}V^{(m)} - \zeta_{11}^{(m+1)}W^{(m)} - \zeta_{3}^{(m+1)}R^{(m)} - \zeta_{7}^{(m+1)}S^{(m)}),\\
W^{(m+1)} &= \varepsilon_{9}^{(m+1)}X^{(m+1)} + \varepsilon_{5}^{(m+1)}Z^{(m+1)} - 2\varepsilon_{6}^{(m+1)}U^{(m)},\\
R^{(m+1)} &= \varepsilon_{14}^{(m+1)}X^{(m+1)} + \varepsilon_{12}^{(m+1)}Z^{(m+1)} - 2\varepsilon_{13}^{(m+1)}U^{(m)},\\
S^{(m+1)} &= \varepsilon_{13}^{(m+1)}(-\zeta_{7}^{(m+1)}V^{(m)} - \zeta_{9}^{(m+1)}W^{(m)} - \zeta_{10}^{(m+1)}R^{(m)} + \zeta_{14}^{(m+1)}S^{(m)}),
\end{aligned}
\tag{26}
$$

where

$$
\begin{aligned}
X^{(m+1)} &= \zeta_{11}^{(m+1)}V^{(m)} + \zeta_{15}^{(m+1)}W^{(m)} - \zeta_{7}^{(m+1)}R^{(m)} + \zeta_{9}^{(m+1)}S^{(m)},\\
Z^{(m+1)} &= \zeta_{8}^{(m+1)}V^{(m)} - \zeta_{7}^{(m+1)}W^{(m)} + \zeta_{12}^{(m+1)}R^{(m)} + \zeta_{10}^{(m+1)}S^{(m)}.
\end{aligned}
\tag{27}
$$

The dispersion function is formed by starting with the real quantities

$$
\begin{aligned}
U^{(0)} &= -\gamma_1(\gamma_1 - 1), \\
V^{(0)} &= 0, \\
W^{(0)} &= (\gamma_1 - 1)^2, \\
R^{(0)} &= \gamma_1{}^2, \\
S^{(0)} &= 0
\end{aligned}
\tag{28}
$$

and by repeated applications of Eqs. (24) or (26), until the dispersion function has been carried down to the (n-1)th interface

$$
\begin{aligned}
&[U^{(n-1)}, iV^{(n-1)}, W^{(n-1)}, R^{(n-1)}, iS^{(n-1)}, -U^{(n-1)}] \\
&\qquad = T^{(0)}F^{(1)}F^{(2)}\cdots \begin{cases} F^{(n-1)} & \text{if } n-1 \text{ is even,} \\ \bar{F}^{(n-1)} & \text{if } n-1 \text{ is odd.} \end{cases}
\end{aligned}
\tag{29}
$$

The complete dispersion function is given by

$$
F_R = [V^{(n-1)}, W^{(n-1)}, R^{(n-1)}, S^{(n-1)}] \begin{cases} \begin{bmatrix} -(1 - c^2/\alpha_n{}^2)^{1/2} \\ -(1 - c^2/\alpha_n{}^2)^{1/2}(1 - c^2/\beta_n{}^2)^{1/2} \\ 1 \\ -(1 - c^2/\beta_n{}^2)^{1/2} \end{bmatrix} \varepsilon & \text{if } n \text{ is even} \\ \begin{bmatrix} (1 - c^2/\beta_n{}^2)^{1/2} \\ 1 \\ -(1 - c^2/\alpha_n{}^2)^{1/2}(1 - c^2/\beta_n{}^2)^{1/2} \\ (1 - c^2/\alpha_n{}^2)^{1/2} \end{bmatrix} \varepsilon & \text{if } n \text{ is odd} \end{cases}
\tag{30}
$$

Since expressions (24)-(28) and (30) involve only real quantities, the use and manipulation of complex numbers is completely avoided in forming the Rayleigh wave dispersion function.

Analogous developments can be made for Earth models containing fluid layers (see, Schwab and Knopoff, 1972).

Once the phase velocity, c, is obtained for a given angular frequency p, the group velocity, u, is obtained from

$$
u = \frac{c}{1-(dc/dp)(p/c)}
\tag{31}
$$

where standard implicit function theory is applied to the dispersion function, $\mathcal{F}_R$, to obtain

$$
\frac{dc}{dp} = -\left(\frac{\partial \mathcal{F}_R}{\partial p}\right)_c \Bigg/ \left(\frac{\partial \mathcal{F}_R}{\partial c}\right)_p
\tag{32}
$$

From Schwab and Knopoff (1972) Eq. (32) can be computed from:

$$
\left(\frac{\partial \mathcal{F}_R}{\partial p}\right)_c = T^{(0)'}\bar{\Lambda}^{(1)} + \sum_{i=1}^{n-1} \begin{cases} \Gamma^{(i-1)}F^{(i)'}\bar{\Lambda}^{(i+1)} & \text{if } i \text{ is even,} \\ \Gamma^{(i-1)}\bar{F}^{(i)'}\Lambda^{(i+1)} & \text{if } i \text{ is odd,} \end{cases}
\tag{33}
$$

$$\left(\frac{\partial \mathcal{F}_R}{\partial c}\right)_{\not p} = T^{(0)}\overline{\Lambda}^{(1)} + \sum_{i=1}^{n-1}\begin{cases}\Gamma^{(i-1)}F^{(i)}\overline{\Lambda}^{(i+1)} & \text{if } i \text{ is even,}\\ \Gamma^{(i-1)}\bar{F}^{(i)}\Lambda^{(i+1)} & \text{if } i \text{ is odd,}\end{cases} + \begin{cases}\Gamma^{(n-1)}\mathcal{F}^{(n)}_{solid} & \text{if } n \text{ is even,}\\ \Gamma^{(n-1)}\bar{\mathcal{F}}^{(n)}_{solid} & \text{if } n \text{ is odd,}\end{cases} \tag{34}$$

where

$$\mathcal{F}_R = F_R/\mathcal{E}\,,\quad \mathcal{F}'^{(n)}_{solid} = T'^{(n)}_{solid}/\mathcal{E}\,,\quad \bar{\mathcal{F}}'^{(n)}_{solid} = \bar{T}'^{(n)}_{solid}/\mathcal{E}\,,$$

primes indicate the operation $(\partial/\partial \not p)_c$, dots, the operation $(\partial/\partial c)$, and

$$\Gamma^{(i-1)} = \begin{cases} T^{(0)} & i-1=0,\\ T^{(0)}F^{(1)}F^{(2)}\cdots F^{(i-2)}F^{(i-1)} & i-1=2,4,6,\ldots,n-1,\\ T^{(0)}\bar{F}^{(1)}F^{(2)}\cdots F^{(i-2)}\bar{F}^{(i-1)} & i-1=1,3,5,\ldots,n-1.\end{cases} \tag{35}$$

If n is even,

$$\Lambda^{(i+1)} = \begin{cases} F^{(i+1)}F^{(i+2)}F^{(i+3)}\cdots F^{(n-1)}\mathcal{F}^{(n)}_{solid} & i+1=2,4,6,\ldots,n-2,\\ \mathcal{F}^{(n)}_{solid} & i+1=n,\end{cases}$$
$$\overline{\Lambda}^{(i+1)} = \bar{F}^{(i+1)}F^{(i+2)}\bar{F}^{(i+3)}\cdots F^{(n-1)}\mathcal{F}^{(n)}_{solid} \quad i+1=1,3,5,\ldots,n-1, \tag{36}$$

and if n is odd,

$$\Lambda^{(i+1)} = F^{(i+1)}F^{(i+2)}F^{(i+3)}\cdots F^{(n-1)}\mathcal{F}^{(n)}_{solid} \quad i+1=2,4,6,\ldots,n-1,$$
$$\overline{\Lambda}^{(i+1)} = \begin{cases} \bar{F}^{(i+1)}F^{(i+2)}\bar{F}^{(i+3)}\cdots F^{(n-2)}F^{(n-1)}\mathcal{F}^{(n)}_{solid} & i+1=1,3,5,\ldots,n-2,\\ \mathcal{F}^{(n)}_{solid} & i+1=n.\end{cases} \tag{37}$$

The elements of the 1x6 matrices $\Gamma^{(i-1)}$ and $\bar{\Gamma}^{(i-1)}$ are obtained by repeated application of (24) and (26) to the initial elements, (28). In order to optimize computation, the elements of $\Lambda^{(i+1)}$ and $\overline{\Lambda}^{(i+1)}$ should be evaluated operating from right to left. Here, the basic interface-matrix multiplication has the form (6x6)(6x1), where the sixth element of the 6x1 matrix is always the negative of the first. The symmetry of the 6x6 matrices, as indicated in (23), is the reason that the 6x1 matrix retains this property throughout the formation of $\Lambda^{(i+1)}$ and $\overline{\Lambda}^{(i+1)}$. This symmetry allows the original six sixth-order multiplications to be replaced by one third-order, and four fifth-order multiplications. After algebraic simplification and combination of the matrix multiplication with the formation of the elements of the new, (m-1)th, 6x6 matrix, the algorithm for the computation of $\Lambda^{(i+1)}$ and $\overline{\Lambda}^{(i+1)}$ takes the following form.

In order to determine the matrices

$$\Lambda^{(l+1)}, \bar{\Lambda}^{(l+1)} = \begin{bmatrix} u^{(l+1)} \\ iv^{(l+1)} \\ w^{(l+1)} \\ r^{(l+1)} \\ is^{(l+1)} \\ -u^{(l+1)} \end{bmatrix}, \tag{38}$$

begin with $u^{(n)}=0$ and, if n is even,

$$\begin{aligned} v^{(n)} &= (1 - c^2/\alpha_n^2)^{1/2}, \\ w^{(n)} &= -(1 - c^2/\alpha_n^2)^{1/2}(1 - c^2/\beta_n^2)^{1/2}, \\ r^{(n)} &= 1, \\ s^{(n)} &= (1 - c^2/\beta_n^2)^{1/2}; \end{aligned} \tag{39}$$

or, if n is odd,

$$\begin{aligned} v^{(n)} &= -(1 - c^2/\beta_n^2)^{1/2}, \\ w^{(n)} &= 1, \\ r^{(n)} &= -(1 - c^2/\alpha_n^2)^{1/2}(1 - c^2/\beta_n^2)^{1/2}, \\ s^{(n)} &= -(1 - c^2/\alpha_n^2)^{1/2}. \end{aligned} \tag{40}$$

Repeated application of (41) or (43) will determine the elements of the desired matrices. If m-1 is even,

$$\begin{aligned} u^{(m-1)} &= -\varepsilon_{16}^{(m-1)}u^{(m)} + \varepsilon_{13}^{(m-1)}w^{(m)} + \varepsilon_{6}^{(m-1)}r^{(m)}, \\ v^{(m-1)} &= -x_1\zeta_{9}^{(m-1)} - x_2\zeta_{10}^{(m-1)} + x_3\zeta_{14}^{(m-1)} - x_4\zeta_{7}^{(m-1)}, \\ w^{(m-1)} &= x_1\zeta_{7}^{(m-1)} - x_2\zeta_{12}^{(m-1)} - x_3\zeta_{10}^{(m-1)} - x_4\zeta_{8}^{(m-1)}, \\ r^{(m-1)} &= -x_1\zeta_{15}^{(m-1)} + x_2\zeta_{7}^{(m-1)} - x_3\zeta_{9}^{(m-1)} - x_4\zeta_{11}^{(m-1)}, \\ s^{(m-1)} &= -x_1\zeta_{11}^{(m-1)} - x_2\zeta_{8}^{(m-1)} - x_3\zeta_{7}^{(m-1)} + x_4\zeta_{13}^{(m-1)}, \end{aligned} \tag{41}$$

where

$$\begin{aligned} x_1 &= 2\varepsilon_{11}^{(m-1)}u^{(m)} - \varepsilon_{14}^{(m-1)}w^{(m)} - \varepsilon_{5}^{(m-1)}r^{(m)}, \\ x_2 &= 2\varepsilon_{7}^{(m-1)}u^{(m)} - \varepsilon_{12}^{(m-1)}w^{(m)} - \varepsilon_{3}^{(m-1)}r^{(m)}, \\ x_3 &= \varepsilon_{15}^{(m-1)}v^{(m)}, \\ x_4 &= \varepsilon_{15}^{(m-1)}s^{(m)}; \end{aligned} \tag{42}$$

and if m-1 is odd,

$$\begin{aligned} u^{(m-1)} &= -\varepsilon_{16}^{(m-1)}u^{(m)} - \varepsilon_{6}^{(m-1)}w^{(m)} - \varepsilon_{13}^{(m-1)}r^{(m)}, \\ v^{(m-1)} &= -y_1\zeta_{11}^{(m-1)} - y_2\zeta_{8}^{(m-1)} + y_3\zeta_{13}^{(m-1)} - y_4\zeta_{7}^{(m-1)}, \\ w^{(m-1)} &= y_1\zeta_{13}^{(m-1)} - y_2\zeta_{7}^{(m-1)} + y_3\zeta_{11}^{(m-1)} + y_4\zeta_{8}^{(m-1)}, \\ r^{(m-1)} &= -y_1\zeta_{7}^{(m-1)} + y_2\zeta_{12}^{(m-1)} + y_3\zeta_{8}^{(m-1)} + y_4\zeta_{10}^{(m-1)}, \\ s^{(m-1)} &= -y_1\zeta_{8}^{(m-1)} - y_2\zeta_{10}^{(m-1)} - y_3\zeta_{7}^{(m-1)} + y_4\zeta_{14}^{(m-1)}, \end{aligned} \tag{43}$$

where

$$\begin{aligned} y_1 &= 2\varepsilon_{11}^{(m-1)}u^{(m)} + \varepsilon_{5}^{(m-1)}w^{(m)} + \varepsilon_{14}^{(m-1)}r^{(m)}, \\ y_2 &= 2\varepsilon_{7}^{(m-1)}u^{(m)} + \varepsilon_{3}^{(m-1)}w^{(m)} + \varepsilon_{12}^{(m-1)}r^{(m)}, \\ y_3 &= \varepsilon_{15}^{(m-1)}v^{(m)}, \\ y_4 &= \varepsilon_{15}^{(m-1)}s^{(m)}. \end{aligned} \tag{44}$$

4. Computation of eigenfunctions

The algorithmic details of eigenfunction evaluation by Knopoff's method are rather involved - although in principle only a straightforward application of Cramer's rule is required - whereas the details for the original formulation (Haskell, 1953) are quite simple. Thus, the programmer's first hope is once a modified formulation has been successfully employed, to compute an eigenvalue at a frequency where this phase velocity was originally unattainable due to precision loss, and then, to reintroduce this eigenvalue into the original formulation to successfully determine the associated eigenfunctions. Unfortunately this approach does not work. It is therefore necessary to employ a modified version of the original formulation for Rayleigh waves also when computing high-frequency eigenfunctions (Schwab et al., 1984).

The problem is the evaluation of the eigenfunctions u(z), w(z), σ(z), and τ(z). In the notation of the previous section, this problem reduces to the determination of the constants A_m, B_m, C_m, D_m for the layers above the homogeneous half-space, and the constants A_n and D_n for this deepest structural unit. Our starting point is therefore the linear, homogeneous system of 4n - 2 equations in 4n - 2 unknowns

$$\begin{bmatrix} \Lambda^{(0)} & & & \\ & \Lambda^{(1)} & & \\ & & \ddots & \\ & & & \Lambda^{(n-2)} \\ & & & & \Lambda^{(n-1)} \end{bmatrix} \begin{bmatrix} & A_1 \\ r_{\alpha 1} & B_1 \\ r_{\beta 1} & C_1 \\ & D_1 \\ & A_2 \\ r_{\alpha 2} & B_2 \\ r_{\beta 2} & C_2 \\ & D_2 \\ & \vdots \\ & A_{n-1} \\ r_{\alpha n-1} & B_{n-1} \\ r_{\beta n-1} & C_{n-1} \\ & D_{n-1} \\ & A_n \\ & D_n \end{bmatrix} = \begin{bmatrix} 0 \\ \\ \\ \\ \\ \\ \\ \\ \vdots \\ \\ \\ \\ \\ \\ 0 \end{bmatrix}, \qquad (45)$$

where the submatrices $\Lambda^{(m)}$ are given by equations (12), (14) and (15). Once the dispersion or eigenvalue problem has been solved by seeking roots of the determinant of the coefficient matrix, we are ready to determine the layer constants. This is done by deleting the last equation of the system and transposing the terms containing D_n to the right-hand side of the equations, thus forming a vector of inhomogeneous terms. If we arbitrarily set D_n to unity, this will force all $r_{\alpha m}B_m$ and D_m to be real, and all A_m and $r_{\beta m}C_m$ to be imaginary. The system now takes the form

$$\begin{bmatrix} & & \\ & & \\ & & \end{bmatrix} \begin{bmatrix} A_1 \\ \vdots \\ r_{\alpha n-1}\, B_{n-1} \\ r_{\beta n-1}\, C_{n-1} \\ D_{n-1} \\ A_n \end{bmatrix} = \begin{bmatrix} 0 \\ \vdots \\ 0 \\ r_{\beta n} \\ -1 \\ \rho_n \gamma_n r_{\beta n} \end{bmatrix}, \tag{46}$$

to which we apply Cramer's rule to obtain

$$A_n = \frac{A_n \Delta_n}{\Delta_n}, \tag{47}$$

where the determinants of the numerator and denominator are expressed as matrix products

$$A_n \Delta_n = T^{(0)} F^{(1)} F^{(2)} F^{(3)} \cdots \begin{cases} F^{(n-2)} T_{A\Delta}^{(n-1)} & \text{if } n-1 \text{ is even} \\ F^{(n-2)} T_{A\Delta}^{(n-1)} & \text{if } n-1 \text{ is odd} \end{cases} \tag{48}$$

$$\Delta_n = T^{(0)} F^{(1)} F^{(2)} F^{(3)} \cdots \begin{cases} F^{(n-2)} T_{\Delta}^{(n-1)} & \text{if } n-1 \text{ is even} \\ F^{(n-2)} T_{\Delta}^{(n-1)} & \text{if } n-1 \text{ is odd.} \end{cases} \tag{49}$$

Following the manipulations described by Schwab (1979, Table 1) and Schwab et al. (1984) it is possible to write

$$[U^{(n-2)}, iV^{(n-2)}, W^{(n-2)}, R^{(n-2)}, iS^{(n-2)}, -U^{(n-2)}] = \frac{1}{\rho_1^{\,2}(\rho_1^{\,2}\rho_2^{\,2} \cdots \rho_{n-2}^{2})\rho_{n-1}} T^{(0)} F^{(1)} \cdots \begin{cases} F^{(n-2)} \\ F^{(n-2)} \end{cases} \tag{50}$$

where U, V, W, R, S are all real. The remaining 6x1 matrices

$$T_{A\Delta}^{(n-1)} = \begin{bmatrix} T_{121}^{A\Delta} \\ T_{131}^{A\Delta} \\ T_{141}^{A\Delta} \\ T_{231}^{A\Delta} \\ T_{241}^{A\Delta} \\ T_{341}^{A\Delta} \end{bmatrix}, \quad T_{A\Delta}^{(n-1)} = \begin{bmatrix} T_{341}^{A\Delta} \\ -T_{241}^{A\Delta} \\ T_{231}^{A\Delta} \\ T_{141}^{A\Delta} \\ -T_{131}^{A\Delta} \\ T_{121}^{A\Delta} \end{bmatrix},$$

$$T_{\Delta}^{(n-1)} = \begin{bmatrix} T_{121}^{\Delta} \\ T_{131}^{\Delta} \\ T_{141}^{\Delta} \\ T_{231}^{\Delta} \\ T_{241}^{\Delta} \\ T_{341}^{\Delta} \end{bmatrix}, \quad T_{\Delta}^{(n-1)} = \begin{bmatrix} T_{341}^{\Delta} \\ -T_{241}^{\Delta} \\ T_{231}^{\Delta} \\ T_{141}^{\Delta} \\ -T_{131}^{\Delta} \\ T_{121}^{\Delta} \end{bmatrix} \tag{51}$$

are formed from the lower, right-hand, 3x5 submatrices of the respective determinants by specifying T^{k}_{ijl} to be the 3x3 determinant made up of the i-th, j-th, and fifth columns, in that order, of the 3x5 submatrices. Thus,

$$T_{\Delta}^{(n-1)} = \begin{bmatrix} \epsilon_4^{(n-1)} \\ i[\epsilon_4^{(n-1)} \zeta_9^{(n-1)} + r_{nn}^{*} \zeta_7^{(n-1)} + \epsilon_3^{(n-1)} \zeta_{10}^{(n-1)}] \\ -\epsilon_4^{(n-1)} \zeta_7^{(n-1)} + r_{nn}^{*} \zeta_8^{(n-1)} + \epsilon_3^{(n-1)} \zeta_{12}^{(n-1)} \\ \epsilon_4^{(n-1)} \zeta_{15}^{(n-1)} + r_{nn}^{*} \zeta_{11}^{(n-1)} - \epsilon_3^{(n-1)} \zeta_7^{(n-1)} \\ i[\epsilon_4^{(n-1)} \zeta_{11}^{(n-1)} - r_{nn}^{*} \zeta_{13}^{(n-1)} + \epsilon_3^{(n-1)} \zeta_8^{(n-1)}] \\ -\epsilon_3^{(n-1)} \end{bmatrix} \tag{52}$$

$$T_{A\Delta}^{(n-1)} = i r_{\beta n}^{*} \begin{bmatrix} -\epsilon_2^{(n-1)} \\ i[-\epsilon_2^{(n-1)} \zeta_9^{(n-1)} - (r_{\beta n}^{*})^{-1} \zeta_7^{(n-1)} - \epsilon_1^{(n-1)} \zeta_{10}^{(n-1)}] \\ \epsilon_2^{(n-1)} \zeta_7^{(n-1)} - (r_{\beta n}^{*})^{-1} \zeta_8^{(n-1)} - \epsilon_1^{(n-1)} \zeta_{12}^{(n-1)} \\ -\epsilon_2^{(n-1)} \zeta_{15}^{(n-1)} - (r_{\beta n}^{*})^{-1} \zeta_{11}^{(n-1)} + \epsilon_1^{(n-1)} \zeta_7^{(n-1)} \\ i[-\epsilon_2^{(n-1)} \zeta_{11}^{(n-1)} + (r_{\beta n}^{*})^{-1} \zeta_{13}^{(n-1)} - \epsilon_1^{(n-1)} \zeta_8^{(n-1)}] \\ \epsilon_1^{(n-1)} \end{bmatrix}, \tag{53}$$

where $\epsilon^{(m)}$ and $\zeta^{(m)}$ are given by Schwab (Table 2, 1970).

To obtain A_{n-1}, $r_{\alpha_{n-1}}$ B_{n-1}, $r_{\beta_{n-1}}$ C_{n-1}, D_{n-1}, equation (46) is further reduced by deleting the last equation of the system and transposing terms including A_n to the right-hand side of the equations

$$\begin{bmatrix} & \\ & \end{bmatrix} \begin{bmatrix} A_1 \\ \vdots \\ A_{n-1} \\ r_{\alpha n-1}B_{n-1} \\ r_{\beta n-1}C_{n-1} \\ D_{n-1} \end{bmatrix} = \begin{bmatrix} 0 \\ \vdots \\ 0 \\ \psi_1^{(n)} \\ \psi_2^{(n)} \end{bmatrix}, \tag{54}$$

In the vector of inhomogeneities, $\psi^{(n)}_1$ is imaginary and $\psi^{(n)}_2$ is real

$$\psi_1^{(n)} = A_n + r_{\beta n} \tag{55}$$

$$\psi_2^{(n)} = r_{\alpha n}A_n - 1. \tag{56}$$

We again apply Cramer's rule to obtain the desired layer constants from

$$\begin{aligned} A_{n-1} &= \frac{A_{n-1}\Delta_{n-1}}{\Delta_{n-1}}, \qquad r_{\alpha n-1}B_{n-1} = \frac{r_{\alpha n-1}B_{n-1}\Delta_{n-1}}{\Delta_{n-1}}, \\ r_{\beta n-1}C_{n-1} &= \frac{r_{\beta n-1}C_{n-1}\Delta_{n-1}}{\Delta_{n-1}}, \qquad D_{n-1} = \frac{D_{n-1}\Delta_{n-1}}{\Delta_{n-1}}, \end{aligned} \tag{57}$$

where, we decompose determinants into products of matrices of the form

$$A_{n-1}\Delta_{n-1} = T^{(0)}F^{(1)}F^{(2)}F^{(3)} \cdots \begin{cases} F^{(n-2)}E^{(n-1)}_{\lambda\lambda} & \text{if } n-1 \text{ is even} \\ F^{(n-2)}\bar{E}^{(n-1)}_{\lambda\lambda} & \text{if } n-1 \text{ is odd} \end{cases} \tag{58}$$

$$\Delta_{n-1} = T^{(0)}F^{(1)}F^{(2)}F^{(3)} \cdots \begin{cases} F^{(n-2)}E_{\lambda}^{(n-1)} & \text{if } n-1 \text{ is even} \\ F^{(n-2)}\bar{E}_{\lambda}^{(n-1)} & \text{if } n-1 \text{ is odd.} \end{cases} \tag{59}$$

Thus we can again use (50) to obtain these products up to the last multiplication on right. The latter 6x1 matrices are formed from the lower, right-hand, 2x4 submatrices of the respective determinants by specifying E^k_{ij} in

$$E^{(n-1)}_{\lambda\lambda} = \begin{bmatrix} E^{\lambda\lambda}_{12} \\ E^{\lambda\lambda}_{13} \\ E^{\lambda\lambda}_{14} \\ E^{\lambda\lambda}_{23} \\ E^{\lambda\lambda}_{24} \\ E^{\lambda\lambda}_{34} \end{bmatrix}, \qquad \bar{E}^{(n-1)}_{\lambda\lambda} = \begin{bmatrix} E^{\lambda\lambda}_{34} \\ -E^{\lambda\lambda}_{24} \\ E^{\lambda\lambda}_{23} \\ E^{\lambda\lambda}_{14} \\ -E^{\lambda\lambda}_{13} \\ E^{\lambda\lambda}_{12} \end{bmatrix}, \tag{60}$$

$$E_{\lambda}^{(n-1)} = \begin{bmatrix} E^{\lambda}_{12} \\ E^{\lambda}_{13} \\ E^{\lambda}_{14} \\ E^{\lambda}_{23} \\ E^{\lambda}_{24} \\ E^{\lambda}_{34} \end{bmatrix}, \qquad \bar{E}_{\lambda}^{(n-1)} = \begin{bmatrix} E^{\lambda}_{34} \\ -E^{\lambda}_{24} \\ E^{\lambda}_{23} \\ E^{\lambda}_{14} \\ -E^{\lambda}_{13} \\ E^{\lambda}_{12} \end{bmatrix}$$

to be the 2x2 determinant made up of the i-th and j-th columns, in that order, of the 2x4 submatrices. Expressions similar to (60) hold for $E^{(n-1)}_{r_\alpha B_\lambda}$, $\bar{E}^{(n-1)}_{r_\alpha B_\lambda}$, $E^{(n-1)}_{r_\beta C_\lambda}$, $\bar{E}^{(n-1)}_{r_\beta C_\lambda}$, $E^{(n-1)}_{D_\lambda}$ and $\bar{E}^{(n-1)}_{D_\lambda}$. Thus

$$E_{AJ}^{(n-1)} = \begin{bmatrix} i[(\psi_1^{(n)})^*\zeta_1^{(n-1)} + \psi_2^{(n)}\zeta_4^{(n-1)}] \\ (\psi_1^{(n)})^*\zeta_6^{(n-1)} - \psi_2^{(n)}\zeta_2^{(n-1)} \\ i[-(\psi_1^{(n)})^*\zeta_2^{(n-1)} + \psi_2^{(n)}\zeta_6^{(n-1)}] \\ \hline \\ \hline \\ \hline \end{bmatrix}, E_{r_m BJ}^{(n-1)}$$

$$= \begin{bmatrix} -(\psi_1^{(n)})^*\zeta_3^{(n-1)} + \psi_2^{(n)}\zeta_1^{(n-1)} \\ \hline \\ \hline \\ -(\psi_1^{(n)})^*\zeta_6^{(n-1)} - \psi_2^{(n)}\zeta_2^{(n-1)} \\ i[-(\psi_1^{(n)})^*\zeta_2^{(n-1)} + \psi_2^{(n)}\zeta_6^{(n-1)}] \\ \hline \end{bmatrix}$$

$$E_{r_m CJ}^{(n-1)} = \begin{bmatrix} \hline \\ -(\psi_1^{(n)})^*\zeta_3^{(n-1)} + \psi_2^{(n)}\zeta_1^{(n-1)} \\ \hline \\ i[-(\psi_1^{(n)})^*\zeta_1^{(n-1)} - \psi_2^{(n)}\zeta_4^{(n-1)}] \\ \hline \\ i[-(\psi_1^{(n)})^*\zeta_2^{(n-1)} + \psi_2^{(n)}\zeta_6^{(n-1)}] \\ \hline \end{bmatrix}, E_{DJ}^{(n-1)} \qquad (61)$$

$$= \begin{bmatrix} \hline \\ \hline \\ -(\psi_1^{(n)})^*\zeta_3^{(n-1)} + \psi_2^{(n)}\zeta_1^{(n-1)} \\ \hline \\ i[-(\psi_1^{(n)})^*\zeta_1^{(n-1)} - \psi_2^{(n)}\zeta_4^{(n-1)}] \\ (\psi_1^{(n)})^*\zeta_6^{(n-1)} + \psi_2^{(n)}\zeta_2^{(n-1)} \end{bmatrix}$$

$$E_J^{(n-1)} = \begin{bmatrix} 1 \\ i[\zeta_9^{(n-1)} + \zeta_{10}^{(n-1)}] \\ -\zeta_7^{(n-1)} + \zeta_{12}^{(n-1)} \\ \zeta_{15}^{(n-1)} - \zeta_7^{(n-1)} \\ i[\zeta_{11}^{(n-1)} + \zeta_8^{(n-1)}] \\ -1 \end{bmatrix}$$

where the neglected terms in the first four matrices need not be considered because they correspond to vanishing elements in the associated left-hand matrix

$$[U^{(n-2)}, iV^{(n-2)}, W^{(n-2)}, R^{(n-2)}, iS^{(n-2)}, -U^{(n-2)}]. \qquad (62)$$

The above scheme can be continued to obtain the remaining layer constants, with the only change being in the definitions of the two elements of the vector of inhomogeneities: for $m < n$,

$$\psi_1^{(m)} = A_m + r_{\beta m} C_m \qquad (63)$$

$$\psi_2^{(m)} = r_{\alpha m} B_m - D_m. \qquad (64)$$

Along with eigenvalues and eigenfunctions, the integral

$$I_4 = \int_0^\infty \rho(z)\left\{\left[\frac{\dot{u}^*(z)}{\dot{w}(0)}\right]^2 + \left[\frac{\dot{w}(z)}{\dot{w}(0)}\right]^2\right\} dz \qquad (65)$$

is required in multi-mode synthesis of theoretical seismograms. For a sequence of homogeneous layers, this integral can be written as

$$I_4 = \begin{cases} c^2\{[r_{\alpha 1}B_1] - [D_1]\}^{-2} \sum_{m=1}^{n} I_{(m)} & \text{for a continental structure} \\ c^2\{[r_{\alpha 1}B_1] - [D_1]\}^{-2} \sum_{m=0}^{n} I_{(m)} & \text{for an oceanic structure,} \end{cases} \qquad (66)$$

where

$$I_{(0)} = \int_{z^{(n-1)}}^{z^{(n)}} \rho_0\{[\dot{u}^*(z)]^2 + [\dot{w}(z)]^2\}\, dz \qquad (67)$$

is given by

$$\frac{\rho_0[r_{\alpha 0}B_0]^2}{2\omega c r_{\alpha 0}}\,[\sin P_0\cos P_0(1 - 1/r_{\alpha 0}^2) + P_0(1 + 1/r_{\alpha 0}^2)]; \tag{68}$$

where

$$I_{m+1} = \int_{z^{(m-1)}}^{z^{(m)}} \rho_m[|\dot{u}^*(z)|^2 + |\dot{w}(z)|^2]\,dz,\ 1 \leq m \leq n-1 \tag{69}$$

is given by

$$\begin{aligned}
\frac{\rho_m}{\omega c}\Bigg\{\frac{1}{2}\Bigg[&\zeta_1^{(m)}\zeta_4^{(m)}(([A_m]^*)^2(1 - r_{\alpha m}^2) + [r_{\alpha m}B_m]^2(1 - 1/r_{\alpha m}^2))\\
&+ \frac{P_m}{r_{\alpha m}}(([A_m]^*)^2(1 + r_{\alpha m}^2) + [r_{\alpha m}B_m]^2(1 + 1/r_{\alpha m}^2))\\
&+ \zeta_2^{(m)}\zeta_6^{(m)}(([r_{\beta m}C_m]^*)^2(1 - 1/r_{\beta m}^2) + [D_m]^2(1 - r_{\beta m}^2))\\
&+ \frac{Q_m}{r_{\beta m}}(([r_{\beta m}C_m]^*)^2(1 + 1/r_{\beta m}^2) + [D_m]^2(1 + r_{\beta m}^2))\Bigg]\\
&+ \zeta_3^{(m)}\zeta_4^{(m)}([A_m]^*[r_{\alpha m}B_m](1 - 1/r_{\alpha m}^2))\\
&- \zeta_5^{(m)}\zeta_6^{(m)}([r_{\beta m}C_m]^*[D_m](1 - 1/r_{\beta m}^2))\\
&+ 2[-\zeta_2^{(m)}\zeta_4^{(m)}[r_{\alpha m}B_m][D_m] + \zeta_1^{(m)}\zeta_6^{(m)}[A_m]^*[r_{\beta m}C_m]^*\\
&+ \zeta_1^{(m)}\zeta_2^{(m)}[A_m]^*[D_m]\\
&- [A_m]^*[D_m] - \zeta_4^{(m)}\zeta_6^{(m)}[r_{\alpha m}B_m][r_{\beta m}C_m]^*]\Bigg\};
\end{aligned} \tag{70}$$

and where

$$I_n = \int_{z^{(n-1)}}^{\infty} \rho_n[|\dot{u}^*(z)|^2 + |\dot{w}(z)|^2]\,dz \tag{71}$$

is given by

$$\begin{aligned}
\frac{\rho_n}{\omega c}\Bigg\{&-\frac{1}{2}([A_n]^*)^2(r_{\alpha n}^* + 1/r_{\alpha n}^*)\\
&-\frac{1}{2}[D_n]^2(r_{\beta n}^* + 1/r_{\beta n}^*) - 2[A_n]^*[D_n]\Bigg\},
\end{aligned} \tag{72}$$

with, of course, D_n specified to be unity.

5. Mode follower and structure minimization

Since all the problems connected with the loss-of-precision at high frequencies have been solved (Schwab, 1970; Schwab et al., 1984; Panza, 1985), the summation of higher modes of surface waves can be used for the generation of "complete" synthetic seismograms also at high frequencies.

The key point in the use of multimode summation is an efficient computation of phase velocity for the different modes at sufficiently small frequency intervals, Δf, and with sufficient precision. To be efficient it is not advisable to determine, at each frequency and for each mode, the zeros of the dispersion function using the standard root-bracketing and root-refininf procedure (e.g. Schwab and Knopoff, 1972). This procedure must be used only when strictly necessary, as for instance at the beginning of each mode. For all other points, i, of each mode the phase velocity can be estimated by cubic extrapolation, using the values of the phase slowness s=1/c and df/ds already determined at frequencies f_{i-2} and f_{i-1}. However the

precision which can be reached in this way is not satisfactory, thus the phase velocity value must be refined. This can be done by an iterative cubic fit in the F-c plane. In our experience, such a procedure has given always highly accurate determinations of the phase velocity and allows a considerable time saving compared with the standard root-bracketing root-refining procedure.

Once the problem of an efficient determination of phase velocities is solved, two other main problems must be solved at each frequency:

a) to correctly follow a mode;

b) to determine the minimum number of layers to be used.

The problem of correctly following a mode arises in the high frequency domain ($f > 0.1$ Hz) where several higher modes are very close to each other. The determination of the minimum number of layers to be used - structure minimization - is critical in order to reach a high precision in phase velocity determination spending the minimum possible computer time.

In order to ensure a high efficiency in the computation of synthetic seismograms, it is necessary to compute the basic ingredients in the frequency domain - phase velocity, phase attenuation, group velocity, energy integral and ellipticity - at constant frequency intervals. To reach a maximum frequency of 10 Hz a satisfactory step

turned out to be 0.05 Hz. To determine the total number of modes present in the frequency interval considered we fix $c_0=0.98\ \beta_n$, where β_n is the S-wave velocity in the half-space, and we increment f, using the Schwab and Knopoff (1972) algorithm to find the values of f corresponding to zeros of the dispersion function $F(f, c_0)$. Obviously, starting from f=0, the first zero in $F(f, c_0)$ corresponds to the fundamental mode, the second to the first higher mode and so on. The values of f for which $F(f, c_0)=0$ are used as starting frequencies (the lowest frequencies) for the computation of the different modes. Once the starting frequency for each mode is defined, it is possible to compute, beginning from the fundamental mode, all dispersion relations. This is accomplished by keeping f fixed and varying c, the procedure being applied at all the equally spaced frequency points of the chosen frequency interval.

5.1 The mode follower

The basic idea is to define an efficient method to follow a given mode M in the phase velocity-frequency space, distinguishing it from the neighbouring modes M-1 and M+1, a problem which is most severe near the osculation points, as, for instance, those characterizing the transition from crustal waves to channel waves (Panza et al., 1972). For frequencies as high as 1 Hz the fundamental mode is in

general well separated from the remaining modes, while for higher frequencies this is no longer true. Thus for the construction of synthetic signals containing high-frequency the mode follower must be applied to all modes, including the fundamental. On the basis of our experience up to now, there are no other modes present in the proximity of the near osculations between the fundamental and the first higher mode. To follow the fundamental mode it is therefore sufficient to use the following properties of $\partial F/\partial c$:

a) for a given mode M, the sign of $\partial F/\partial c$ is constant with frequency;

b) going from a mode to the next $\partial F/\partial c$ changes sign with regularity.

In other words, once the sign of $\partial F/\partial c$ is computed at the initial frequency of the fundamental mode, in all subsequent points the simple check of this sign makes it possible to follow the mode correctly. In fact, with increasing frequency, as long as the sign of $\partial F/\partial c$ does not change, the obtained zero of F(f, c) belongs to the fundamental mode. If the sign of $\partial F/\partial c$ changes, the zero of F(f, c) does not belong to the fundamental mode and the search of the zero restarts from a lower value of c. In such a way it is possible to compute all the dispersion curve for the fundamental mode quite rapidly.

For the higher modes the above algorithm is not

sufficient because they are generally much closer to each-other. However the construction of an efficient mode follower is still possible.

In fact, as can be deduced from the work of Tolstoy (1956), for a given higher mode, even if computations are made for structures containing very strong low-velocity layers, the phase velocity decreases with increasing frequency. Thus for each higher mode, M, the possible value of the phase velocity, at a given frequency f, lies in the range (c_1, c_2), where c_1 is the phase velocity of the mode M-1 at the frequency f and c_2 is the phase velocity of the mode M at the frequency $f-\Delta f$. If the computations are carried to a maximum frequency of 1 Hz we suggest a frequency step $\Delta f=0.005$ Hz, while if the maximum frequency is 10 Hz then $\Delta f=0.05$. This condition, combined with the property of the sign of $\partial F/\partial c$ recognizes an eventual jump from mode M to modes $M+(2n+1)$ $(n=0,1,\ldots)$. If in the domain (c_1, c_2) and $(f-\Delta f, f)$ $2m+1$ $(m=1,2,\ldots)$ modes are contained, the procedure just outlined is not sufficient to follow the mode. On the basis of our experience we can state that this happens very seldom; thus we have not bothered to derive a very efficient algorithm to solve this problem. Our mode follower recognizes this mode jump only when the computation of modes M+1 and M+2 is completed. At this point the computation can be restarted from the mode M at the

frequency f using as the initial phase velocity a value just slightly greater than that of the mode M-1 at the same frequency.

Even if up to now we have carried out computations for a limited sample of continental and oceanic structural models (Panza, 1985; Chiaruttini, Costa and Panza, 1985), we can state that this version of the mode follower is totally satisfactory to compute with high efficiency all the frequency domain ingredients of synthetic seismograms.

5.2 Structure minimization

The structure minimization is a critical point regarding the efficiency and the accuracy of the computation of eigenvalues, eigenfunctions and related quantities. In order to save computer time, it is necessary to determine for each frequency, the minimum amount of structure to be used in the computation, while retaining very high accuracy. In general for a structure made by n layers this can be done by computing the quantity

$$E_m = \bar{\rho}_m \left[\left(\frac{u_m^*}{w_o} \right)^2 + \left(\frac{w_m}{w_o} \right)^2 \right] \qquad m=1,\ldots n-1 \qquad (73)$$

where

$$\bar{\rho}_m = \frac{\rho_{m-1} + \rho_m}{2} \qquad \text{if} \quad m \geq 2$$

and ρ_{m-1} and ρ_m are the densities in layers m-1 and m, if m=1 $\bar{\rho}_1 = \rho_1$.

Since we have chosen for each mode to start from the lowest frequencies consistent with a value of $c=0.98\,\beta_n$, the amount of structure to be used at the beginning of each mode coincides with the total number, n, of layers in the structural model. Once the phase velocity is determined, E_m can easily be computed and starting from m=n-1 it is easy to locate its deepest minimum value.

At this stage all the layers below the interface, j, corresponding to the deepest minimum value of E_m can be discarded and the parameters of the j+1 layer are used to define the half-space. With the minimized structure it is now possible to compute with the necessary accuracy, more than 8 figures, the final value of the phase velocity. In general, repeating this procedure for each frequency and for each mode gives very satisfactory results.

Particular care must be placed in the structure minimization when low velocity layers are present in the structural model. Let us consider here the case of only one low velocity channel, the extension to many velocity inversions being quite obvious. For the waves propagating essentially in the low velocity channel, the necessary accuracy is ensured by simply placing the terminating half-space just below the zone of velocity inversion. For

the waves propagating above the low velocity channel, i.e. for the waves with a phase velocity less than the minimum S-wave velocity in the channel, only the structure above the deepest minimum of E_m located above the channel needs to be retained.

The situation is completely different when dealing with waves propagating with a phase velocity larger than the minimum S-wave velocity in the channel, i.e. for waves mainly propagating above the low velocity channel but sampling also deeper. For these waves it is generally necessary to keep at least all the channel, assigning the properties of the layer immediately below it to the half-space. It must be observed that in many cases the penetration in the low velocity channel is so small, that the structure minimization can be performed, without loosing in precision, by removing the whole channel, with evident time saving. The identification of the waves for which the above reduction is possible can be made by evaluating E_m, starting at m=0. If in some of the layers just above the low velocity layer $E_j \leq 10^{-4} E_o$, then the structure can be terminated at the j-th interface, using as half-space characteristics those of the j-th layer. From the description given above it is clear that the initial amount of structure used for the computation at a given frequency, f, is determined by the result of the structure minimization

at the frequency f-Δf. This is obviously not valid if at the frequency f-Δf there was a wave sampling the channel very weakly ($E_j < 10^{-4} E_o$). In these cases the amount of structure initially used at the frequency, f, contains always the low velocity layer.

6. Attenuation due to anelasticity

The anelastic nature of the Earth's interior manifests itself through the phenomena of attenuation of elastic waves. Knopoff (1964b) introduced an additional term into the differential equation of motion to account for attenuation effects. He introduced the nondimensional constant Q, which is related to the space ($e^{-\alpha x}$) and time ($e^{-\gamma t}$) attenuation coefficients as follows

$$\alpha = \frac{p}{2Qc} \qquad \gamma = \frac{p}{2Q} \tag{74}$$

where c is the phase velocity of the plane wave motion under consideration. Recently, O'Connell and Budiansky (1978) derived the relation

$$Q = \frac{1}{2}\left(\frac{p}{\alpha c} - \frac{\alpha c}{p}\right) \tag{75}$$

which is relevant only for small values of p (long-period waves and free oscillations). Brune (1962) and Knopoff et

al. (1964) noted that there are some discrepancies for Q obtained from propagating wave trains, Q_x, and that from free oscillations, Q_t. The two values are joined by the relation $uQ_t=cQ_x$ where c and u are phase and group velocity, respectively.

The following discussion of a way in which dissipation of wave energy can be taken into account in seismogram calculations is tailored directly to the needs of seismology. The literature on anelastic and rheological properties of earth materials is very vast. As a starting point for the interested reader, we mention only a book by Christensen (1982) on viscoelasticity in general and a review article by Minster (1980) which is geophysically oriented.

Dissipation or absorption of wave energy is often described by linear laws, i.e. it is assumed that stress and strain are linearly related as in purely elastic media. The difference to this case is that now phase shifts occur between stress and strain. This implies that the elastic moduli are no longer real, but complex and possibly frequency dependent. The simple one-dimensional stress-strain relation is

$$\sigma(p) = M(p)\epsilon(p). \qquad (76)$$

If ϵ is a shear strain, σ a shear stress, then M is identical with twice the complex rigidity μ. If ϵ is a volume strain or cubic dilatation, σ a pressure (apart from the sign), then M is the complex bulk modulus k. As a third example, if ϵ is the strain along a rod or wire, σ the corresponding uniaxial stress, then M is the complex Young's modulus. We will call M(p) the viscoelastic modulus without specifying the mode of deformation. The general three-dimensional viscoelastic stress-strain relation of an isotropic substance is

$$\sigma_{ij}(p) = [k(p)-\frac{2}{3}\mu(p)]\theta(p)\delta_{ij}+2\mu(p)\epsilon_{ij}(p), \qquad (77)$$

where θ is the cubic dilatation and otherwise familiar notation has been used.

The viscoelastic modulus in Eq. (76) is separated into real and imaginary parts, $M=M_1+iM_2$, or into magnitude and phase, $M=Ae^{i\phi}$. All these quantities in principle have to be considered as frequency dependent. The quality factor Q is defined by

$$Q^{-1} = M_2/M_1 = \tan\phi\ . \qquad (78)$$

Increasing dissipation increases the phase shift ϕ between stress and strain and hence decreases Q. It can be shown

that, if $Q \gg 1$, Q^{-1} is proportional to the energy loss per period in a harmonic loading experiment and therefore has a simple physical meaning. Q can be measured by different techniques, including amplitude measurements of propagating waves, width measurements of spectral lines in spectra of free oscillations and, of course, phase-shift measurements between stress and strain in forced oscillations.

An important point to note is that Eq. (76), and similarly Eq. (77), can be considered as a linear filter equation. The filter, represented by the viscoelastic modulus, must be causal, i.e. the filter output $\sigma(t)$ in the time domain must not start earlier than the filter input $\epsilon(t)$. This requirement imposes relations between M_1 and M_2, or A and ϕ, which are called dispersion or Kramers-Kronig relations. Those relating magnitude A and phase ϕ (and hence Q, according to Eq. (78)) are the most important in the present context:

$$\ln A(p) = B - \frac{1}{\pi} P \int_{-\infty}^{+\infty} \frac{\phi(p')}{p'-p}\, dp' \qquad (79)$$

$$\phi(p) = \frac{1}{\pi} P \int_{-\infty}^{+\infty} \frac{\ln A(p')}{p'-p}\, dp' \,. \qquad (80)$$

Here only Eq. (79) is needed. For simple types of frequency dependence of Q, the principal-value integral can be calculated analytically and the constant B can be determined

either at high or at low frequencies. As a consequence the viscoelastic modulus is known for all frequencies. If this procedure is followed for the rigidity $\mu(p)$ and the bulk modulus k(p), and if these complex moduli are used instead of the real moduli in the solution of an elastic wave-propagation problem, then the frequency-domain solution of the corresponding viscoelastic problem is obtained. This is the correspondence principle of the linear theory of viscoelasticity. The time-domain solution of the viscoelastic problem follows as usual by inverse Fourier transformation.

Working with $\mu(p)$ and k(p) is, however, not the procedure that is normally used. Rather, one works with wave velocities and hence replaces real velocities by complex velocities. For P and S waves, we have the complex velocities

$$\alpha_c(p) = \left[\frac{M_\alpha(p)}{\rho}\right]^{\frac{1}{2}}, \qquad \beta_c(p) = \left[\frac{M_\beta(p)}{\rho}\right]^{\frac{1}{2}}, \qquad (81)$$

where ρ is the (real) density. The viscoelastic modulus for P waves is

$$M_\alpha(p) = k(p) + \frac{4}{3}\mu(p) \qquad (82)$$

with the quality factor Q_α following from

$$Q_\alpha^{-1} = \frac{4\beta^2}{3\alpha^2} Q_\mu^{-1} + (1 - \frac{4\beta^2}{3\alpha^2}) Q_k^{-1} \quad . \tag{83}$$

For S waves we have, accordingly:

$$M_\beta(p) = \mu(p) \tag{84}$$

$$Q_\beta = Q_\mu \quad . \tag{85}$$

Q_μ and Q_k are the quality factors of μ and k, and α and β in Eq. (83) are real wave velocities taken for a typical frequency. A familiar assumption is $Q_k >> Q_\mu$, i.e. that there is much less dissipation in volume deformation than in shear deformation. Then Q_α depends only on Q_μ, and Q_α and Q_β have the same frequency dependence. In effect this implies a real, frequency-independent bulk modulus, at least in the seismic frequency band. An often used relation is $Q_\alpha = 2.25 Q_\beta$, corresponding to $\alpha^2 = 3\beta^2$.

The procedure to find the complex velocities (81) is to make assumptions about Q_α and Q_β as functions of frequency, to use Eqs. (78) and (79) for the determination of M_α and M_β and then to insert these moduli into Eq. (81). In the following we will again disregard the distinction of P and S waves and work with M(p), Q(p) and the complex velocity

$$v_c(p) = \left[\frac{M(p)}{\rho}\right]^{\frac{1}{2}} \quad . \tag{86}$$

If Q is a frequency-independent constant, or if it follows from the power law

$$Q(p) = Q(p_o)\left(\frac{p}{p_o}\right)^\gamma \tag{87}$$

with the reference frequency p_o and an exponent γ between -1 and +1, the steps leading to the complex velocity (86) are rather straightforward (Müller, 1983) and will not be repeated here. These Q laws and related absorption-band models have been investigated many times in the literature (for a review, see Minster, 1980), although often with unnecessary complications such as cut-off frequencies introduced for mathematical convenience alone. Here we give the results for the case of seismological interest, $Q >> 1$. If Q is constant, this condition applies for all frequencies, and in the case of the power law (87) we consider only frequencies for which $Q >> 1$. In the constant-Q case one obtains the well-known result

$$v_c(p) = v\left(1 + \frac{1}{\pi Q} \ln \frac{p}{p_o} + \frac{i}{2Q}\right) , \tag{88}$$

and in the case of the power law (87)

$$v_c(p) = v\left\{1+\frac{1}{2}\left[\frac{1}{Q(p_o)}-\frac{1}{Q(p)}\right]\right.$$

$$\left.\cot\frac{\gamma\pi}{2}+\frac{i}{2Q(p)}\right\}. \qquad (89)$$

In these expressions, v is a real velocity. The real part of the complex velocity,

$$A_1(p) = \mathrm{Re}\, v_c(p), \qquad A_1(p_o) = v, \qquad (90)$$

is the phase velocity of body-wave propagation. This follows from the plane-wave expression

$$u(x,t) = \exp\{ip(t-\frac{x}{v_c(p)})\}$$

$$= \exp\{ip(t-\frac{x}{A_1(p)(1+\frac{i}{2Q})})\} \qquad (91)$$

$$= \exp\{ip(t-\frac{x}{A_1(p)})\}\exp\{-\frac{px}{2A_1(p)Q}\},$$

which represents a wave with phase velocity $A_1(p)$. The imaginary part of the complex velocity is responsible for absorption, since it leads to the exponential decay of the wave amplitudes in Eq. (91) with increasing propagation

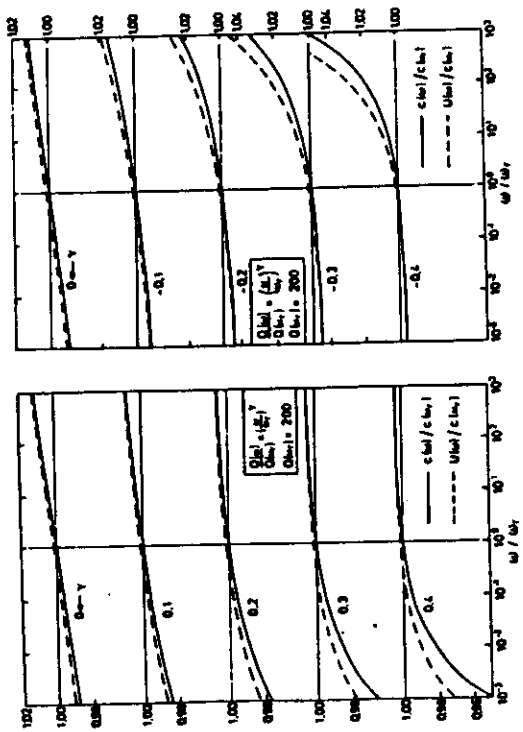

Fig. 3 Relative dispersion for phase velocity c and group velocity U of body waves, corresponding to power laws for the quality factor Q with positive and negative exponents. The case $\gamma = 0$ represents frequency-independent Q

distance x.

The frequency dependence of $A_1(p)$ reflects the dispersion that is connected with absorption. Dispersion is slight, of course, and both positive and negative exponents γ lead to an increase of phase velocity with frequency (Fig. 3).

In a medium with a constant Q, the correction to the dispersion of body waves can be expressed (Futtermann, 1962 eq. (25))

$$A_1(p) = A_1(p_o)/\{1+[\frac{2}{\pi} A_1(p_o)A_2(p_o)\ln(p_o/p)]\},$$
$$B_1(p) = B_1(p_o)/\{1+[\frac{2}{\pi} B_1(p_o)B_2(p_o)\ln(p_o/p)]\}, \qquad (92)$$

where $A_1(p)$ is the P-wave phase velocity, $A_2(p)$ is the P-wave phase attenuation, $B_1(p)$ is the S-wave phase velocity and $B_2(p)$ is the S-wave phase attenuation.

In the following computations we have choosen $p_o=2\pi$ radians. The quantities A_1, A_2, B_1, B_2 are related to the complex body-wave velocities and B, describing the properties of anelastic media, by

$$\frac{1}{\alpha} = \frac{1}{A_1} - iA_2 , \qquad \frac{1}{\beta} = \frac{1}{B_1} - iB_2 \qquad (93)$$

(Schwab and Knopoff, 1972). In anelastic media also surface-wave phase velocity, c, must be expressed as a complex

quantity

$$\frac{1}{c} = \frac{1}{C_1} - iC_2 \quad . \qquad (94)$$

The attenuated phase velocity C_1 and the phase attenuation C_2 can be estimated by using the variational technique (e.g. Takeuchi and Saito, 1972; Aki and Richards, 1980). As an intermediate step it is necessary to compute the integrals

$$I_3 = \int_o^{\infty}\{[(\lambda+2\mu)-\frac{\lambda^2}{(\lambda+2\mu)}]y_3^2 + \frac{1}{k}(y_1y_4-\frac{\lambda}{(\lambda+2\mu)}\ y_2y_3)\}dz \qquad (95)$$

$$I_4 = \int_o^{\infty}\{\delta(\lambda+2\mu)[\frac{1}{(\lambda+2\mu)^2}(y_2^2+2k\lambda y_2y_3) + k^2\{1+\frac{\lambda^2}{(\lambda+2\mu)^2}\}y_3^2\ ] + \delta\mu\frac{1}{\mu^2}y_4^2+\delta\lambda[\frac{2k}{(\lambda+2\mu)}(y_2y_3+k\lambda y_3^2)]\}dz \ , \qquad (96)$$

where

$$y_1 = \frac{w(z)}{w(o)} \qquad y_2 = \frac{\sigma(z)}{w(o)}$$

$$iy_3 = \frac{u(z)}{w(o)} \qquad iy_4 = \frac{\tau(z)}{w(o)}$$

In these expressions, $\bar{\alpha}$ and $\bar{\beta}$ are the compressional- and shear-wave velocities in the perfectly elastic case; in other words

$$\rho(\beta_1+i\beta_2)^2 = \mu+\delta\mu \qquad \rho(\alpha_1+i\alpha_2)^2 = (\lambda+2\mu)+\delta(\lambda+2\mu) \ ,$$

with λ and μ indicating Lamé's constants.

Integrals I_3 and I_4 can be computed analytically from the layer constants (Schwab et al., 1986), thus obtaining the anelastic phase velocity

$$C_1 = \bar{c}/[1- \frac{1}{2\bar{k}^2 I_3} \mathrm{Re}(I_4)] \qquad (97)$$

and the phase attenuation

$$C_2 = \frac{1}{2p\bar{k}I_3} \mathrm{Im}(I_4) \ , \qquad (98)$$

where $\bar{c}$ and $\bar{k}$ are the phase velocity and wavenumber in the perfectly elastic case.

The exact mathematical treatment of attenuation due to anelasticity is described by Schwab and Knopoff (1971, 1972, 1973).

As we have seen, body waves are dispersed in anelastic media. The frequency dependence of body waves requires the introduction of a small but essential variation in the mode follower.

In the perfectly elastic case, for each higher mode, M, the possible value of the phase velocity, at a given

frequency, lies in the range (c_1, c_2). When body wave dispersion is present, the upper limit c_2 has to be redifined. The phase velocity of body waves, in fact, increases with increasing frequency and this may cause an increase of the phase velocity of higher modes with frequency. This effect is evident in those parts of the mode curves which are almost undispersed in the perfectly elastic case. One has therefore to estimate the increase in phase velocity of a given mode at a given frequency f, with respect to the frequency f-Δf, due to the dispersion of body waves.

Let us denote by Δc_2 the maximum possible increment of c_2.

When using Eq. (92) it is convenient to express the difference Δc in the phase velocity between the frequencies f-Δf and f, due to the effect of the body wave dispersion, by

$$\Delta c = \frac{c(f)}{1+x \ln \frac{f_0}{f-\Delta f}} \cdot \frac{x \ln \frac{f}{f-\Delta f}}{1+x \ln \frac{f_0}{f}} \qquad (99)$$

with

$$x = \frac{2}{\pi} c(f) \, C_2(f)$$

The use of (99) is not straightforward, since the value of

Due to body wave dispersion, care must also be taken in computing group velocities using implicit function theory (Eq. 31-32). When computing $\left(\frac{\partial \mathcal{F}_R}{\partial p}\right)_*$ one has to remember that body wave velocities are functions of frequency. In this case equation (33) contains terms associated with the derivative with respect to the angular frequency, p, of the compressional and shear wave velocities.

The effects of body wave dispersion are not very relevant in practice, however we want to stress that the introduction of body waves dispersion in anelastic media is a physical necessity.

7. Response to buried sources

Ben-Menahem and Harkrider (1964) developed the formalism necessary for the study of point sources in multilayered media. The confusion concerning the equivalent forces needed to replace a displacement dislocation was removed by Burridge and Knopoff (1964). To avoid any additional confusion which may arise concerning this point, we will be as explicit as possible in our use of equivalent forces.

We take, as a reasonable model of the earthquake, a non-propagating jump in displacement across the fault plane, with continuous normal stresses across this plane.

Burridge and Knopoff (1964) considered the problem of the force which would have to be applied in the absence of the fault to produce the same radiation pattern as a given dislocation. They found that the equivalent forces which must be applied depend only upon the source mechanism and elastic properties of the medium in the immediate vicinity of the fault, and not upon any reflecting surfaces or other inhomogeneities which may be present in the medium. For the earthquake model we have selected, the equivalent force in a locally homogeneous medium is the double couple without moment.

In Fig. 4(a), a fault is shown before and after dislocation. The fault plane is the plane of separation between the two blocks. The dislocation is described in cartesian co-ordinates in Fig. 4(b), where x_1 and x_2 lie in the fault plane, and x_3 is perpendicular to it; x_1 is parallel to the displacement on the fault. The jump in displacement, u, can be written as in the figure, using the notation of Burridge and Knopoff (1964). Fig. 4(c) shows the equivalent point forces for an unfaulted medium. The quantity $e_1(x,t)$ represents the couple whose forces act in the x_3 direction.

In Fig. 5 we show a co-ordinate system associated with the free surface; the presence of the fault plane is included to connect this co-ordinate system with the actual

Δc depends upon $c(f)$ and $C_2(f)$, quantities which are obviously unknown at this stage of the computation.

In order to estimate Δc one can substitute to $c(f)$ and $C_2(f)$ a weighted average of the S-wave velocities, B_1, and the S-wave phase attenuations, B_2. As weights we use the eigenfunctions at the frequency $f-\Delta f$, in particular the sum of the squared displacements. Therefore

$$\Delta C_2 = \frac{\bar{B}_1(f-\Delta f)}{1-\bar{x}\ \ln \frac{f_o}{f-\Delta f}} \cdot \frac{\bar{x}\ \ln \frac{f}{f-\Delta f}}{1+\bar{x}\ \ln \frac{f_o}{f}} \qquad (100)$$

with

$$\bar{x} = \frac{2}{\pi}\ \bar{B}_1(f-\Delta f)\ \bar{B}_2(f-\Delta f)$$

It has been found with extensive numerical testing that the above relations yield a very satisfactory definition of the upper limit c_2. In the case the wave at the frequency $f-\Delta f$ penetrates to a much smaller depth than that at the frequency f, as for instance in the channel wave - crustal wave sequence, the weighted averages B_1 and B_2 are computed at the last frequency $f-N\Delta f$, where the wave reaches about the same penetration depth as that at the frequency f. The main advantage of the above modification consists in keeping the general scheme of the perfectly elastic mode-follower the same.

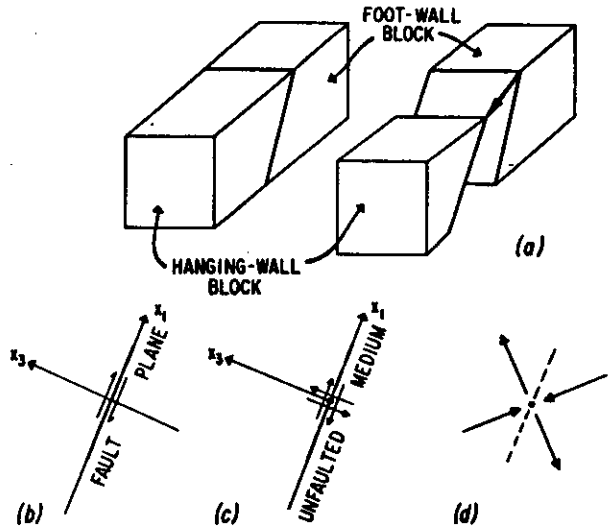

$[u_1]=\delta(x_1)\delta(x_2)H(t)$, $\sigma_1(\vec{x},t)=-\mu\delta(x_1)\delta(x_2)\delta'(x_3)H(t)$

$[u_2]=0, [u_3]=0$ $\sigma_2(\vec{x},t)=0$

$\sigma_3(\vec{x},t)=-\mu\delta'(x_1)\delta(x_2)\delta(x_3)H(t)$

Fig. 4. Fault model of an earthquake and equivalent point-force replacement in an unfaulted medium.

faulting. The quantity h is the depth of the focus, θ is the azimuth of the station with respect to the strike line, δ is the dip angle, λ is the slip angle, and s represents the direction of the displacement dislocation of the hanging wall relative to the foot wall.

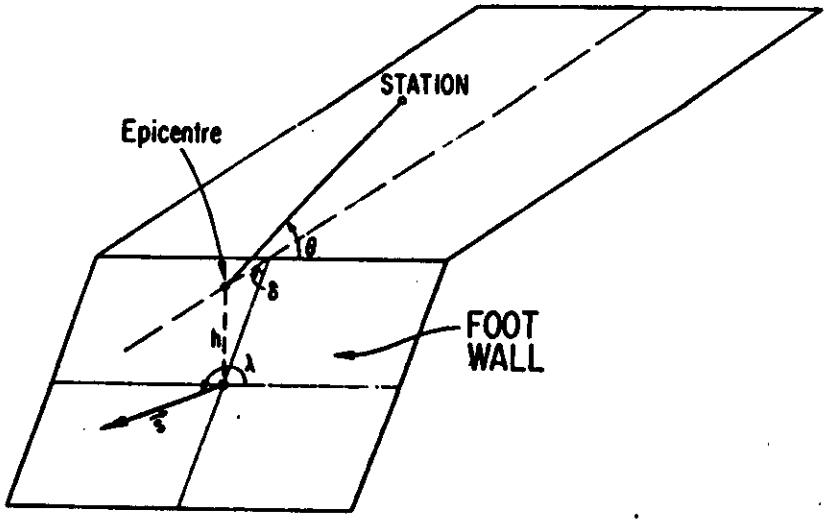

Fig. 5. Source geometry and co-ordinate system associated with free surface.

We consider the radiation pattern for the double couple in order to obtain the surface wave response at the free surface for the various modes.

For a vertical point-force singlet at depth h, the vertical and radial components of the Rayleigh wave displacement at the free surface are given by Harkrider (1964). For the j-th mode, the dependence upon r is just $H^{(2)}_0(k_j r)$ or $H^{(2)}_1(k_j r)$. Harkrider (1964) also gives the response to a horizontal point-force singlet. This case

involves the radial dependence $H^{(2)}_1(k_j r)/k_j r$, as well as those above. The response to a singlet of arbitrary orientation is obtained by a suitable linear combination of the response to a vertical and a horizontal singlet. There is therefore no change in the form of the radial dependence of the response.

The Rayleigh wave response to a point-force couple is obtained from the singlet response by differentiating the latter in the direction of the moment arm, which is normal to the fault plane; and the double-couple response, U^{DC}, is obtained by superposition of two perpendicular couples. Since some of the terms in the double-couple response will involve differentiation of the singlet response with respect to r, it follows that the radial dependence of the components of U^{DC} involves only the factors $H^{(2)}_0$, $H^{(2)}_1$, $H^{(2)}_0/r$, $H^{(2)}_1/r$, and $H^{(2)}_1/r^2$.

If we assume that the receiver is at a sufficiently large distance from the epicentre, we can neglect terms which fall off more rapidly than $r^{-\frac{1}{2}}$ and consider only the first term of the asymptotic expansions of the Hankel functions. This will give us the displacement in the far field. Fig. 6 shows how large a value of kr is needed to obtain an accuracy of σ significant figures in the moduli and arguments (or phases) of $H^{(2)}_0$ and $H^{(2)}_1$. The accuracy σ is given by

$$\sigma = \log_{10}(5|\epsilon|) \qquad (101)$$

where ϵ is the fractional error involved in the use of only the first term of the asymptotic expansion. From Fig. 6 we see that we must have $kr \gtrsim 10$ for 3-figure accuracy in all the amplitudes and arguments.

For $\sigma = 3$ significant figures, the safe distance-period relationship is also given in this figure for the first four Rayleigh wave modes. For example, for the first higher mode, at a period of 100 s, we must limit ourselves to distances greater than 1000 km from the epicentre. This ensures 3-figure accuracy in the computation of the radially-dependent factors in U^{DC} when we use only the first terms of the asymptotic expansions.

In our analysis we use only these first terms to obtain the Fourier time transform of the Rayleigh wave displacement at the free surface:

$$U_r^{DC} = (|R(\omega)|\exp(i\phi_o))|\vec{n}|k^{\frac{1}{2}}\exp(-i3\pi/4)x(\theta,h)\epsilon_o G\exp(-ikr)/\sqrt{(2\pi r)} \qquad (102)$$

$$U_z^{DC} = (\epsilon_o\exp(i\pi/2))^{-1}U_r^{DC} \qquad U_\theta^{DC} = 0$$

where $R(\omega)$ is the Fourier transform of the equivalent point-force time function, the quantity $\vec{n}$ is the unit vector

perpendicular to the fault and has units of length,

$$\phi_o = \arg R(\omega) \qquad (103)$$

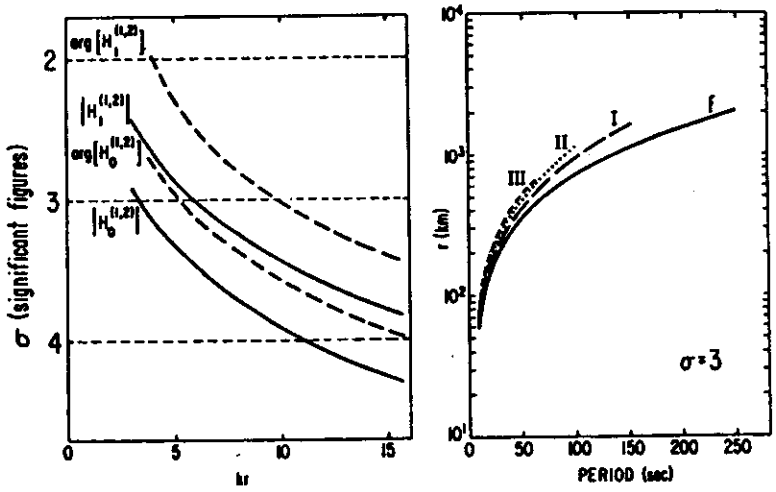

Fig. 6. Accuracy of the first term of the asymptotic expansion of $H^{(1,2)}_1(kr)$ as a function of kr, and minimum value of r for which the first term of the expansion ensures three significant figures in $\arg\,[H^{(1,2)}_1(kr)]$. The latter is given for the fundamental and first three higher Rayleigh wave modes associated with the shield model given by Panza et al. (1972).

is the initial phase, k is the wave number,

$$\epsilon_0 = - \frac{u^*_0}{w_0} \tag{104}$$

The factor G is given by

$$G^{-1} = 2 c u I_1 \tag{105}$$

where

$$I_1 = \int_0^\infty \rho(z)[y_1^2(z)+y_3^2(z)]dz \tag{106}$$

and $\rho(z)$ is the density. The azimuthal dependence of the response is given by

$$X(\theta,h) = d_0+i(d_1\sin\theta+d_2\cos\theta)+d_3\sin2\theta+d_4\cos2\theta \tag{107}$$

where θ is the angle between the strike of the fault and the epicenter-station direction; h is the hypocentral depth. The quantities d_i $(i=0,\ldots,4)$ are

$$\begin{aligned} d_0 &= \tfrac{1}{2}\sin\lambda\sin2\delta B(h) & d_3 &= \cos\lambda\sin\delta A(h) \\ d_1 &= -\sin\lambda\cos2\delta C(h) & d_4 &= -\tfrac{1}{2}\sin\lambda\sin2\delta A(h) \\ d_2 &= -\cos\lambda\cos\delta C(h) \end{aligned} \tag{108}$$

where λ is the rake angle and δ is the dip angle. Furthermore,

$$A(h) = - \frac{u^*(h)}{w_0}$$

$$B(h) = -(3-4\frac{\beta(h)^2}{\alpha(h)^2})\frac{u^*(h)}{w_0} - \frac{2}{\rho(h)\alpha(h)^2}\frac{\sigma^*(h)}{\dot{w}_0/c} \tag{109}$$

$$C(h) = - \frac{1}{\mu(h)}\frac{\tau(h)}{\dot{w}_0/c}$$

where $\alpha(h)$ is the P-wave velocity at the source depth, $\beta(h)=(\mu(h)/\rho(h))^{\frac{1}{2}}$ is the S-wave velocity at the source depth, $u^*(h)$, $\sigma^*(h)$ and $\tau(h)$ are the eigenfunctions at the source depth, w_0 is the vertical displacement at the free surface.

If one adopts the far-field relation given by Ben-Menahem and Harkrider (1964):

$$\frac{U_r}{U_z} = \epsilon_0 e^{i\pi/2} \tag{110}$$

then for a wave propagating in the positive r direction with retrograde elliptical particle motion, U_r leads U_z by $\pi/2$ radians and ϵ_0 is positive only if z is chosen to increase upward. If, however, as in Panza et al. (1972), Haskell (1953), and the first part of Harkrider (1964), z is chosen positive downward, U_r leads U_z by $3\pi/2$ radians. If relation

(110) is used to define ϵ_0, retrograde particle motion will be defined by negative values of the ellipticity. In relation to the formalism given by Ben-Menahem and Harkrider (1964) the following observation is relevant for programming. Since the depth-dependent quantities $u^*(h)/\dot{w}_0$, $c\,\sigma^*(h)/\dot{w}_0$, and $c\,\tau(h)/\dot{w}_0$ are to be computed from the usual Haskell (1953) formalism, in which z is positive in the downward direction, U_r must lead U_z by $3\pi/2$ radians.

The asymptotic expression just described allows the computation of synthetic seismograms with at least 3 significant figures as long as $kr \geq 10$ (Panza et al., 1973), and it is equivalent to the expression in terms of the seismic moment (e.g. see Eqs. (7.149) and (7.150) of Aki and Richards, 1980).

When considering anelastic models, the wave number k is complex

$$k = (p/C_1) - ipC_2 \qquad (111)$$

thus the term exp(-ikr) in (102) can be written as

$$\exp(-ipr/C_1)\exp(-pC_2r) \qquad (112)$$

The term $e^{-\omega C_2 r}$, representing the amplitude damping, is the main term introduced by anelasticity. Smaller

effects, like the ones arising from complex group velocities and eigenfunctions, are not included in the present calculations. We think that they may become important when the problem of lateral variations treatment will be solved.

The extension of these results to the available formalism for sources with finite dimensions and durations is quite straightforward. In case the source is not instantaneous but has a finite rise time, the derivative of the time source function changes from a delta function to a triangular like function of duration T, with the effect of smoothing periods smaller than T.

Finite length sources can be dealt in two ways. In case the source receiver distance is much bigger (at least a factor of 10) than the source dimensions, the Ben-Menahem (1961) factor

$$\frac{\sin X}{X} e^{-iX} \qquad (113)$$

with

$$X = \frac{pL}{2}\left[\frac{1}{v} - \frac{\cos\psi}{c}\right]$$

where p is the angular frequency, L is the source length, v is the rupture velocity, c is the phase velocity and ψ is the azimuth of the station measured from the rupture

direction, may be used, as described in detail by Båth (1974). A second possibility is to compute the seismogram as a sum of point sources shifted in space and time. This last method has been extensively used in connection with empirical Green's functions (e.g. Hartzell, 1978; Kanamori, 1979).

The seismogram $S(t,r)$ at the receiver R due to the extended fault Σ can be expressed as

$$S(t,\bar{r}) = \iint_{\Sigma} s(t+\tau(\bar{r}');\bar{r}-\bar{r}')w(\bar{r}')d\bar{r}' \qquad (114)$$

where s is the response at the receiver R due to a point source at the point r' on the fault Σ and w is a weighting or scaling factor with inverse area units. τ is a time expressing the delay at the point r' due to the rupture propagation and is equal to $|r'|/v$ for a rupture propagating with a constant velocity v.

Since we sum discrete point sources, the integral in (114) will be replaced by a sum

$$S(t,\bar{r}) = \sum_j s_j(t+\tau_j;\bar{r}_j)w'_j \qquad (115)$$

where j runs over the point sources on the fault plane Σ and w'_j is now non-dimensional. This equation is equivalent to Eq. (1) in Hartzell (1978)

$$S(t,\bar{r}) = \Sigma[s_j(t)*Q_j(t)]H(t-\tau_j) \qquad (116)$$

where the (*) indicates convolution, $Q_j(t)$ is a generalized scaling factor (a delta function with a given amplitude in the simplest case), and H indicates the Heaviside step function.

When the successive excitation of regularly spaced point sources is used to approximate a rupture propagation, the apparent time separation between point sources, as seen at the receiver, must be smaller than the Nyquist period of the synthetic signals. In case just a few point sources, approximating irregularly spaced asperities, are considered, the above condition obviously does not have to be satisfied.

It is also quite important to note that the expressions for sources of finite dimensions are valid in the far-field approximation, which can be roughly expressed by the condition that the source-receiver distance must be an order of magnitude greater than the source dimensions. If this condition is not satisfied while the condition $kr \geq 10$ still holds, the synthetic signal can be constructed as proper sum of seismograms given by point sources separated in time and space. With the modal approach this is easily done, since, for a given Earth model, different seismograms corresponding to different sources, can be computed with

very little computer time, essentially the time required for a fast Fourier transform, since all the time consuming computations (eigenvalues and eigenfunctions) are independent from source specifications.

8. Comparison with real data

To show how suitable our method for the summation of Rayleigh wave modes is in modeling observational data, we present in this chapter some examples.

8.1 Borrego Mountain, California, 1968 event

First we try to synthetize the recordings of the Carder displacement meter of the station El Centro (ELC) for the Borrego Mountain, California, M = 6.4 earthquake of April 9, 1968 as given by Heaton and Helmberger (1977).

An atempt to model this earthquake in terms of addition of surface wave modes has been done by Swanger and Boore (1978). These two authors were able to reproduce the transversal component of motion quite well, but failed to obtain a good fit for the radial and vertical component.

The initial structure, BORN, used in the computations (Suhadolc and Panza, 1985) is taken, for what regards the crustal layers (Table II), from the structure used by Swanger and Boore (1978). The mantle part is taken from the models proposed by Biswas and Knopoff (1974) for

TABLE II

Thickness (km)	Density (g/cm^3)	P-wave velocity (km/s)	S-wave velocity (km/s)	Q_β
0.25	2.0	1.7	1.0	20
0.30	2.2	2.1	1.2	30
1.35	2.2	2.4	1.4	40
0.95	2.4	3.3	1.9	100
1.65	2.5	4.3	2.5	200

Structure BORN used in the Borrego Mountain earthquake modeling. Only the uppermost layers are shown. For the remaining structure see Suhadolc and Panza (1985). It has been assumed that $Q_\alpha = 2.5\ Q_\beta$.

the Western United States.

In the initial step of fitting the radial component we held the structure fixed and varied only some of the source parameters. At the beginning we used a single point source model, while later on a two-point model is shown to give a better fit.

8.1.1 Single-point source

The radial and vertical components of the observed displacements are shown in Figs. 7a and 7b respectively. For the source parameters we adopted the ones given by Burdick and Mellman (1976). These authors modeled the teleseismic P pulse by adding the contribution of three point sources occurring in the time span of about 15 s. We used the parameters of the first of these three events, which are also in good accord with the values proposed by Allen and Nordquist (1972). A Heaviside step function was used for the source time function.

The synthetic seismogram obtained with these parameters and the sum of 218 modes is shown in Fig. 8a; its peak half-amplitude is 6.1×10^{-26} cm, thus to obtain the observed maximum displacement of about 3 cm we need a seismic moment of about 12×10^{25} dyne-cm.

It is evident that the amplitude of the observed coda is much larger than the one of the synthetic. This

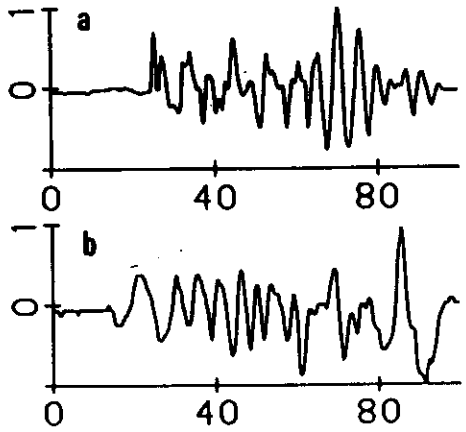

Fig. 7. Observed ground motion due to the Borrego Mountain, California, 1968 earthquake, recorded at El Centro. a) Radial component, maximum zero-to-peak amplitude about 7.3 cm. b) Vertical component, maximum zero-to-peak amplitude about 3.1 cm (after Swanger and Boore, 1978).

problem may be removed by a variation in the depth of the source, which greatly affects the relative amplitudes between the early and late parts of the recording. The synthetics obtained with a source depth of 4.5 km and leaving the other parameters the same, is shown in Fig. 8b. The improvement is quite evident. The bigger excitation of Rayleigh waves in the sedimentary surficial layers, which is probably responsible for the high amplitude late arrivals, is accomplished by a shallower source. The high frequencies present in the early arrivals of the synthetic seismogram of Fig. 8b can be filtered out by using a finite rise time source function. We adopted a symmetric triangular function for the derivative of the source time function. The resulting synthetic for a duration of 2 s is shown in Fig. 8c.

The principal difference seen between the synthetic and the observed recording is still in the amplitudes. The amplitudes of the later arrivals dominate in the observed recording, while in the synthetic the early arrivals are the bigger ones.

To reduce further the ratio between the early and later arrivals we tried to increase the Q factor in the sediments and to diminish it in the crust, obtaining a very small improvement.

For a better fit some structural parameters have to

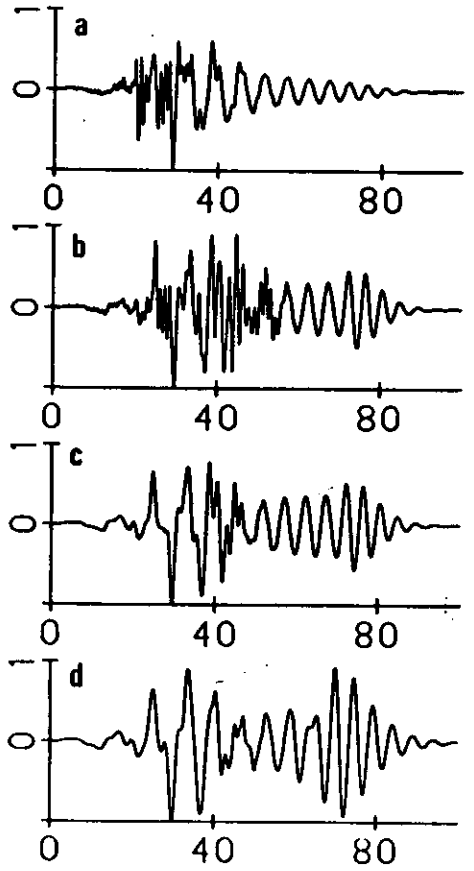

Fig. 8. Single point-source radial component synthetic seismograms referring to the Borrego Mountain 1968 earthquake: parts a, b, c refer to the structure BORN (see Table II and text), while part d refers to the structure BORY (see Table III). The parameters of the sources are described in the text.

be changed. In particular we note that the frequency of the fundamental mode, which produces the large amplitude later arrivals, is lower in the observed seismogram than in the synthetic one. This can be taken care of by increasing the thicknesses of the uppermost layers. After some trials in adjusting the corresponding velocities in order to mantain the correct arrival times, the crustal structure, BORY, shown in Table III was found to give satisfactory results. We note incidentally that the variations in the structural parameters are not very large, however they are required by the data; this may give an idea of the resolving power connected with the use of complete signals. The synthetic displacement corresponding to the structure of Table III, for a source duration of 3 s, is given in Fig. 8d. The fit on the later arrivals is now quite good. The corresponding seismic moment is about 9×10^{25} dyne-cm, in good accord with the values given by Swanger and Boore (1976) and Heaton and Helmberger (1977).

The discrepancies which persist between observed and synthetic data are in the still too large early arrivals, the initial double peak and the latest arrival, which have not been synthetized up to now. The problem can be resolved considering more than one point source.

TABLE III

Thickness (km)	Density (g/cm^3)	P-wave velocity (km/s)	S-wave velocity (km/s)	Q_β
0.50	2.0	1.70	1.00	150
0.25	2.2	2.30	1.35	150
0.25	2.2	2.45	1.45	150
1.60	2.2	2.70	1.60	150
0.55	2.4	3.30	1.90	80
1.35	2.5	4.30	2.50	80

Structure BORY used in the Borrego Mountain earthquake modeling. Only the uppermost layers are shown. For the remaining structure see Suhadolc and Panza (1985). It has been assumed that $Q_\alpha = 2.5\ Q_\beta$.

8.1.2 Two-point source

An easy way to reduce the amplitudes of the first arrivals is to consider more than one point source. Also Heaton and Helmberger (1977), Ebel and Helmberger (1982) and Burdick and Mellman (1976) admit that the event cannot be modeled with a single point source. In order to preserve the good-fitting later arrivals and change only the early part of the synthetic shown in Fig. 8d, a second deeper point source is considered. Since the early arrivals show more high frequency content, a source 8 km deep with a time duration of 1 s was chosen. The seismogram is shown in Fig. 9a. The effect of the sum of the two point sources, the deeper one being 6 s late with respect to the shallower one (Fig. 9b), is shown in Fig. 9c. The weights of the two point sources were chosen to be identical, thus the seismic moment of each source can be estimated around 1.1×10^{26} dyne-cm.

The other features could be modeled assuming more point sources located at different hypocentres, but the problem has not been dealt with in this paper, since it is not our aim to do a particular study of the Borrego Mountain event.

The corresponding synthetic vertical component - the observed one is shown in Fig. 7b - is shown in Fig. 10. The overall fit is not bad at all, but the latest arrivals of the observed recording show sharp phase changes and very big

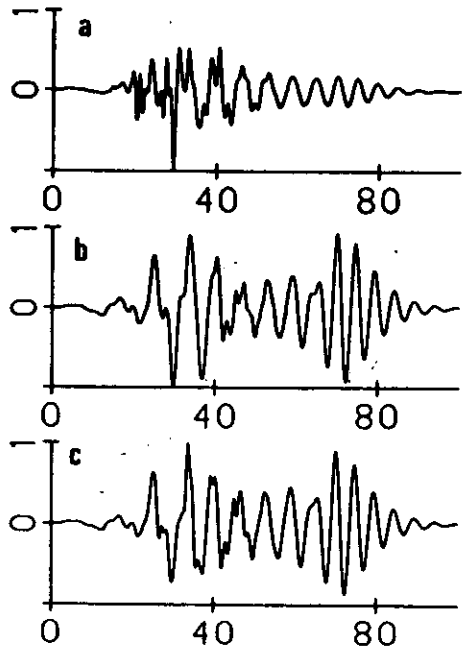

Fig. 9. Two point sources superposition, radial component. a) 8 km deep point source, duration 1 s. b) 4.5 km deep point source, duration 3 s. c) Superposition of the two previous point-sources.

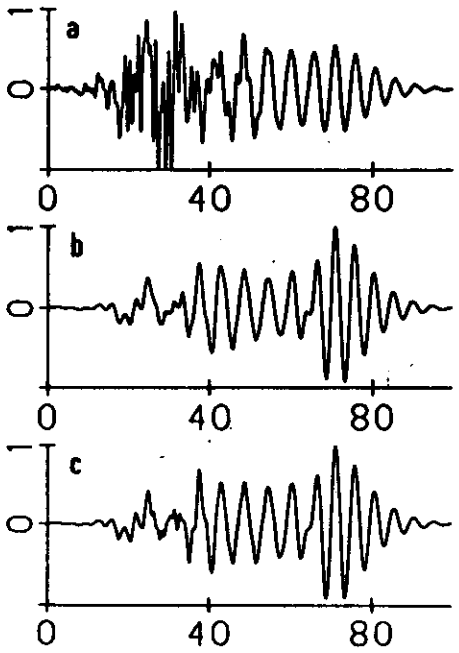

Fig. 10. Same as Fig. 9 for the vertical component.

periods and amplitudes, features missing in the synthetics of Fig. 10. These are very probably due to interference of more point sources and to the effect of lateral variations. Any further attempt to model this component seems to us useless since the size of the first part of the signal, only about one third of the radial, is just above the noise level and thus any later phase arising from lateral variations can become a dominant feature in the record.

8.2 Brawley, California, 1976 event

Strong motion displacements due to the November 4, 1976 Brawley, California earthquake, magnitude 4.9, recorded at the stations El Centro (ELC) and Imperial Valley College (IVC), as given by Heaton and Helmberger (1978) are modeled next. The initial part of the tangential components of these recordings were modeled by Heaton and Helmberger (1978) using the Cagniard-de Hoop technique. Here we will concentrate on the radial components (Fig. 11).

The recorded horizontal ground motion is much larger than the vertical one and the radial displacement at ELC is about a factor of two bigger than at IVC, which lies near a P-SV node. The radial components at the two stations show a high degree of overall coherence, only the relative amplitudes of the single peaks are quite different. This is to be expected, since, assuming the USGS determined

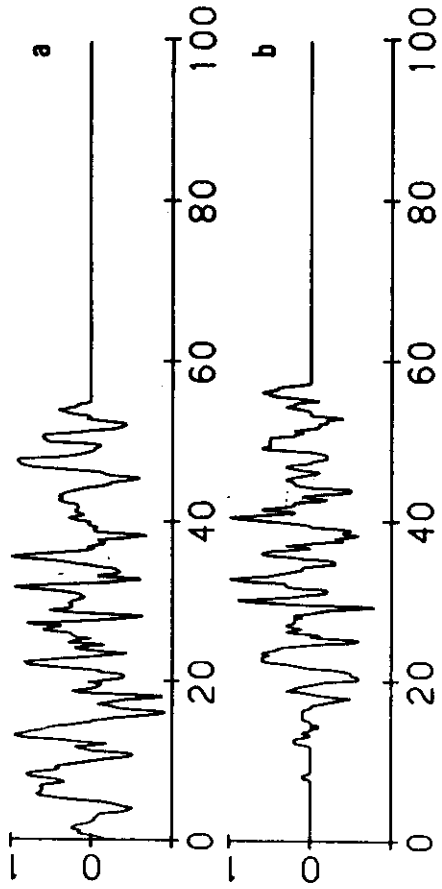

Fig. 11. Observed ground motions, radial component, due to the Brawley, California, 1968 earthquake. a) El Centro (ELC) recording, maximum zero-to-peak amplitude about 1.4 mm. b) Imperial Valley College (IVC) recording, maximum zero-to-peak amplitude about 0.7 mm.

epicenter, the stations have very similar azimuths (160° and 174° for IVC and ELC respectively) and distances (33 km and 36 km) from the source. The hypocentral depth, according to USGS, is 4.5 km. The mechanism determined from local stations first arrivals is a right-lateral strike-slip on a plane dipping almost vertically.

The uppermost five low-velocity layers used in our structural model BRAW (Table IV) are those given by Biehler, Kovach and Allen (1964), while other crust and upper mantle specifications are practically the same as those used in the Borrego Mountain earthquake modeling.

A single point source with a right lateral strike-slip mechanism on a vertical fault plane 7 km deep and with a source duration of 1 s was found to have a much too big initial peak and a too short duration as compared to the observed ELC seismogram. Shallower sources have been therefore tried and a relatively good match obtained with a source 3.5 km deep (Fig. 12a).

Nevertheless the signal duration is still too short. Since a certain degree of coherence has been observed between the initial and the final part of the seismogram, another similar shallow source has been applied 17 s after the first source (Fig. 12c). In order to match the central part another point source, this time 7 km deep and 14.3 s after the first source, has been added (Fig. 12b). The three

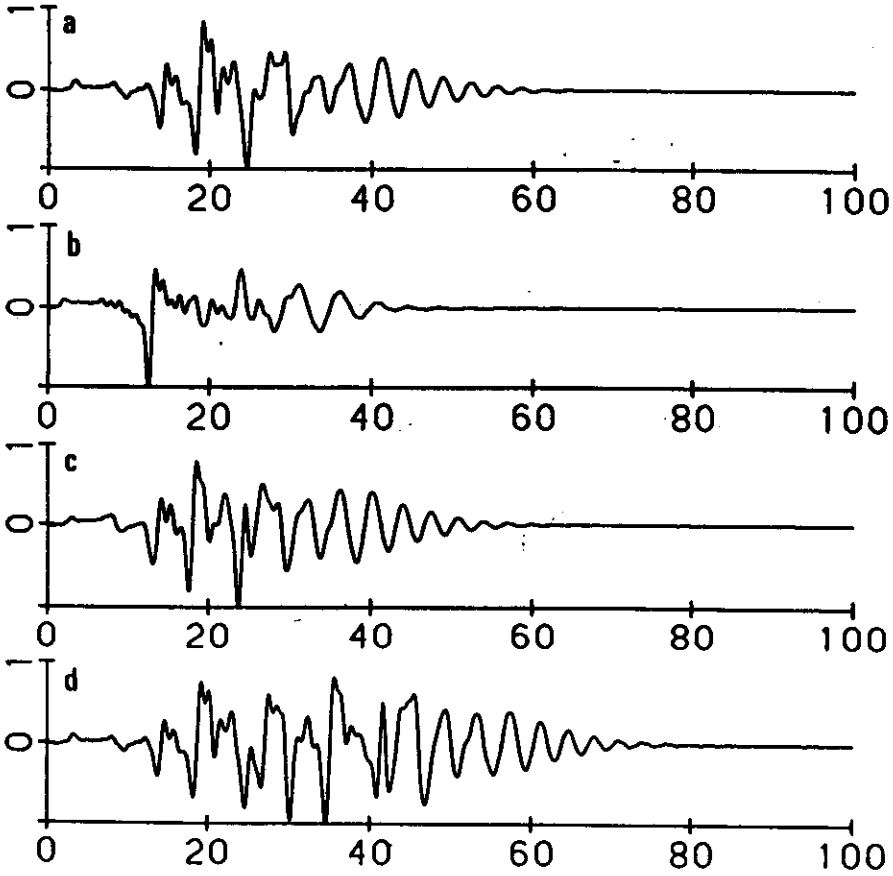

Fig. 12. Synthetic seismograms referring to the Brawley 1976 event and to El Centro (ELC) station. a) 3.5 km deep point source, epicentral distance of 38 km. b) 7 km deep point source, epicentral distance of 36 km. d) Superposition of seismograms a), b) and c). See text for details.

TABLE IV

Thickness (km)	Density (g/cm^3)	P-wave velocity (km/s)	S-wave velocity (km/s)	Q_β
0.45	2.0	1.7	0.75	20
0.50	2.2	2.1	0.92	20
1.15	2.3	2.6	1.50	30
1.30	2.4	3.7	2.13	100
2.50	2.6	4.7	2.71	200

Structure BRAW used in the Brawley earthquake modeling. Only the uppermost layers are shown, the remaining structure being practically identical as in BORY. It has been assumed that $Q_\alpha = 2.5\ Q_\beta$.

sources and their sum - all have been given equal weight - are shown in Fig. 12 for ELC and Fig. 13 for IVC. In order to preserve the relative amplitudes of the initial and final part of the seismogram at both stations, the fault dip of the second shallow source has been set to 80°. The second and the third event are placed at the USGS epicenter, while the first one is placed about 3 km to the northwest, along the fault line. This was seen to give a better fit on the initial part of the record compared with the records (see Figs. 14 and 15) obtained by summing, in the same way as in the former example, three point sources - 3.5 km, 7 km and 3.5 km deep - with the same epicenter (coinciding with the USGS one) and focal mechanism.

It is interesting to note that the epicenter location is pretty well determined to lie along the fault passing through the epicenter given by USGS (33° 05'N, 115° 36°W) by the ratio of the amplitudes at the two stations. This ratio was found to maximize for a vertical fault and for shallow sources.

In the first part of the seismogram the fit of the IVC record is a little bit worse than the ELC one, but the overall features are still reproduced pretty well. Also in this case the small amplitude of the signal can make relevant the effect of lateral variations which may be responsible of the main observed discrepancies. The seismic

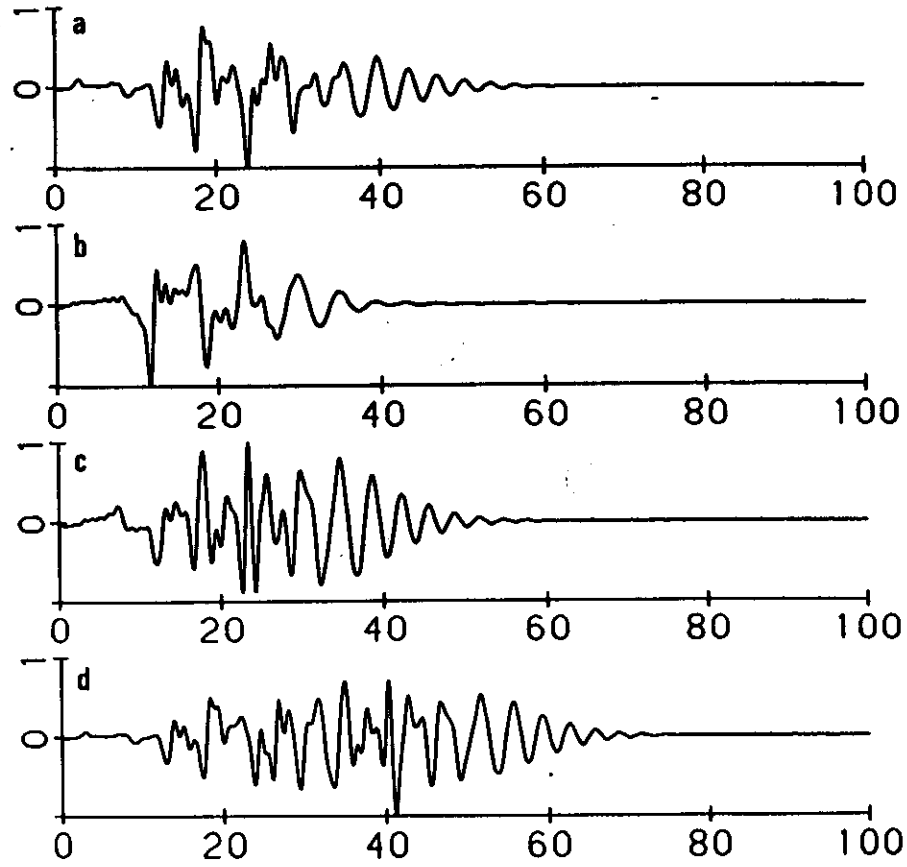

Fig. 13. Same as Fig. 12 for station Imperial Valley College (IVC).

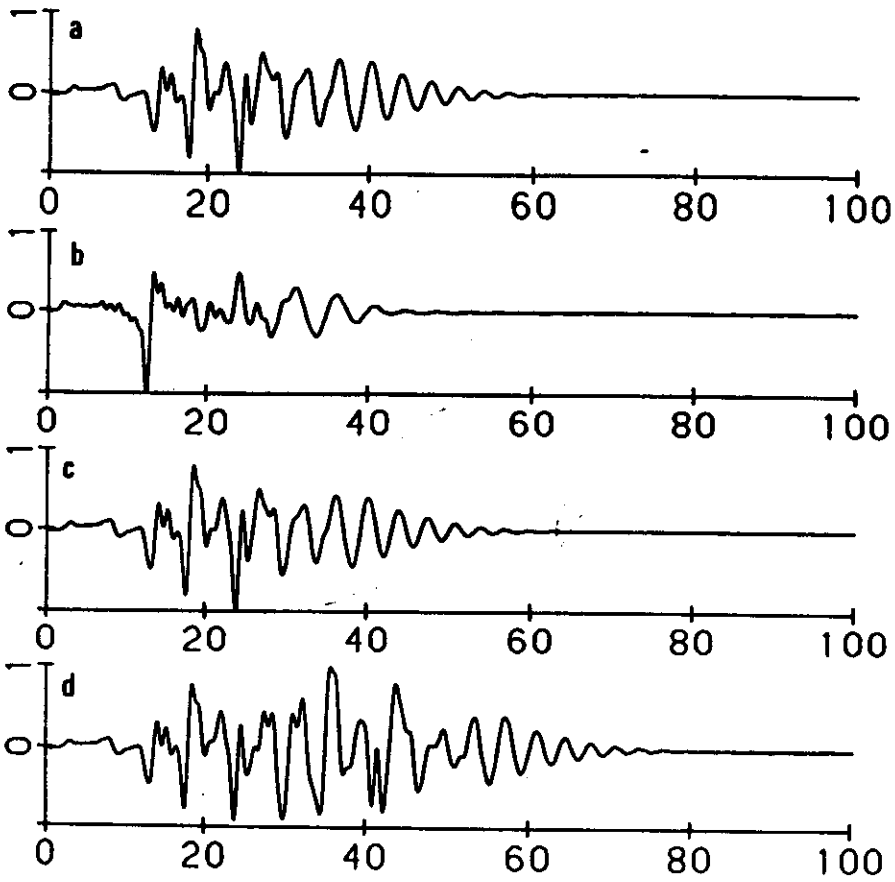

Fig. 14. Same as Fig. 12, the epicentral distance of all the three single point sources being now 36 km.

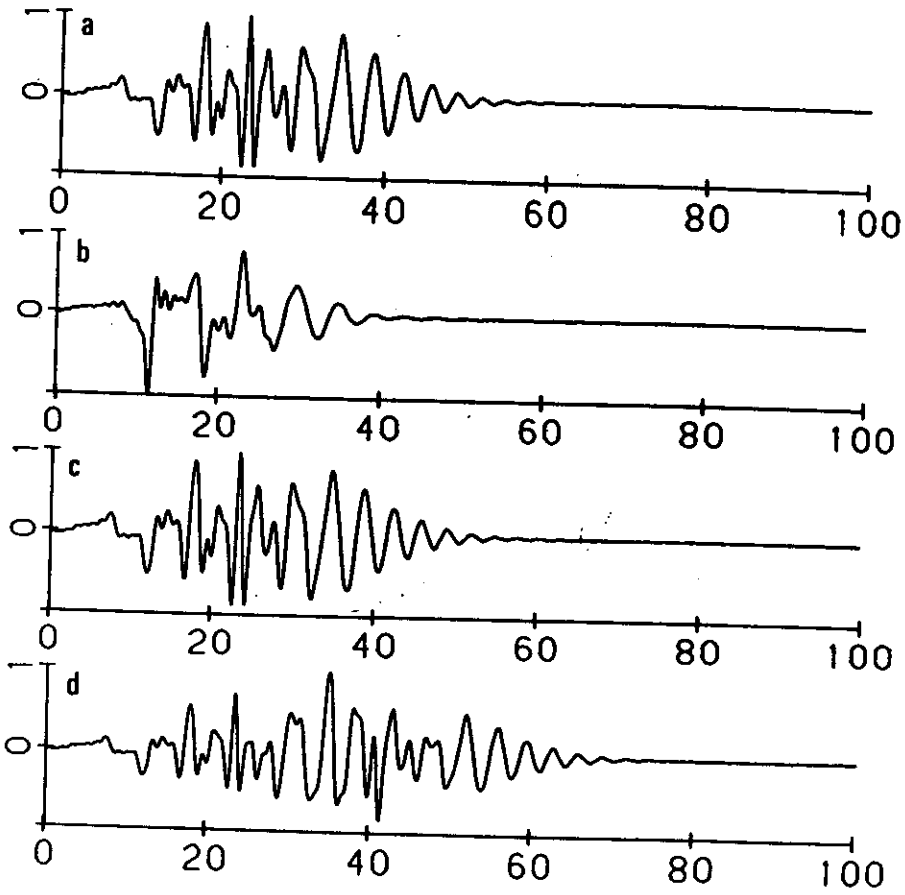

Fig. 15. Same as Fig. 14 for station Imperial Valley College (IVC).

moment of each point source is found to be about 7 x 10^{23} dyne.cm, Heaton and Helmberger (1978) found a value 3 x 10^{23} dyne.cm.

8.3 Irpinia, Italy, 1980 event

The earthquake source behavior is relatively well understood by waveform matching synthetic and observed ground motions for frequencies up to 1. Hz, some examples having been shown in the previous sections. If we move to higher frequencies, smaller scale details of the earthquake source process on one hand and of the structure surrounding the source volume on the other, become essential for a deterministic prediction of the strong ground motion. Since these details are not known at present, a statistical approach has been taken up to now to predict ground motion above 1 Hz (e.g. Boore and Joyner, 1978; Boatwright, 1982; Koyama, 1985).

In the following we present a first attempt to model deterministically some of the ENEA-ENEL strong ground motion recordings (Berardi, Berenzi and Capozza, 1981) of the 1980 Irpinia, Italy, earthquake, M_S = 6.9 (see Deschamps and King (1983) and Del Pezzo, Iannaccone, Martini and Scarpa (1983) for a review of the source parameters of this event).

By just comparing the durations of the observed ground motions (Fig. 16) with those of the synthetic

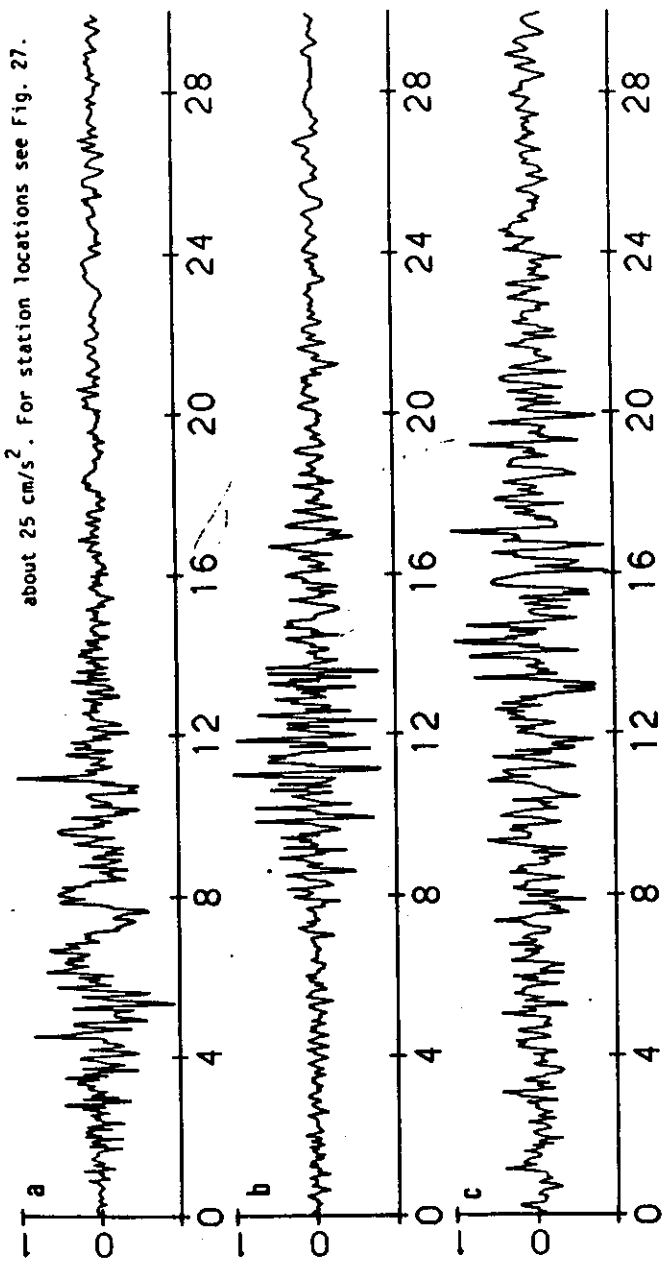

Fig. 16. Observed accelerations, after gaussian-filtering at 10 Hz, due to the Irpinia, Italy, 1980 earthquake. a) Station Sturno, maximum peak ground acceleration about 132 cm/s^2. b) Station Brienza, maximum peak ground acceleration about 83 cm/s^2. c) Station Auletta, maximum peak ground acceleration about 25 cm/s^2. For station locations see Fig. 27.

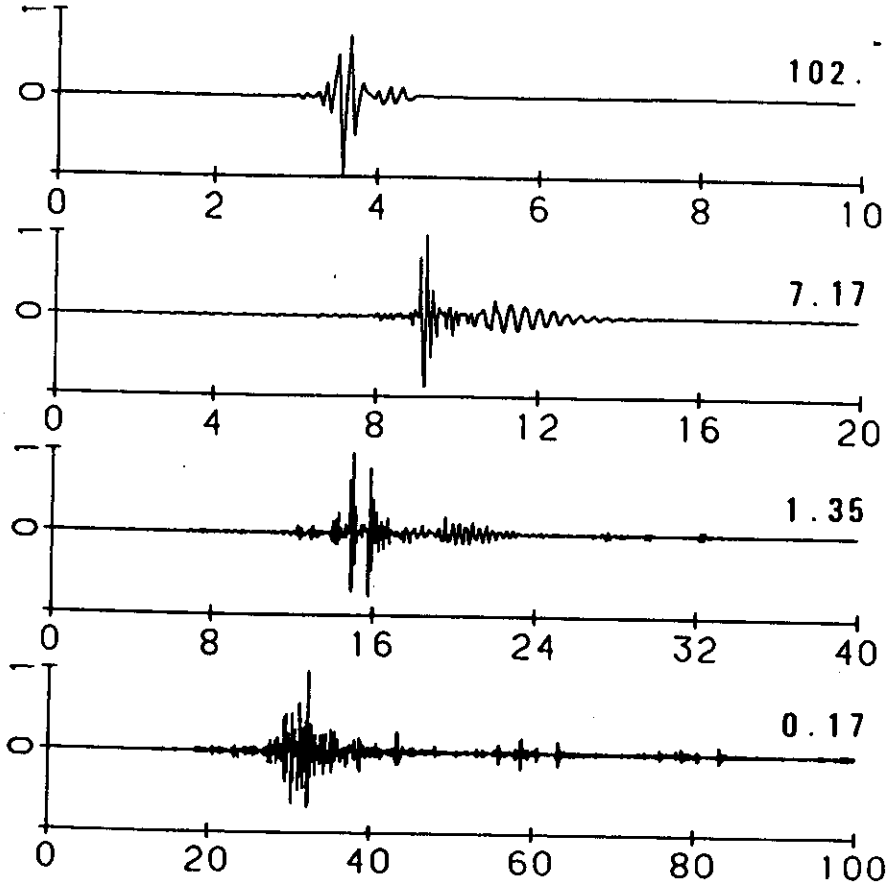

Fig. 17. Vertical component of acceleration for an istantaneous point source (h = 6 km, θ = 68°, δ = 15°, λ = 75°) with seismic moment $|M_o|$ = 1 dyne cm as a function of epicentral distance, r; from top to bottom r = 10, 30, 50, 100 km. The maximum zero-to-peak amplitudes are normalized to one. In this and all subsequent figures the number above each seismogram gives the peak acceleration (here in units of 10^{-22} cm/s^2) and on the horizontal axis the time is given in seconds.

examples, computed at comparable distances (Fig. 17), one can immediately see that a single point source is by no means a realistic representation of the source process. On the basis of our experience most of the observed signal can be reproduced by superposition of point sources, modeling asperities. When the location and rupture time of these asperities is determined by rough waveform fitting, then it is possible to model a more detailed finite dimension fault rupture along the lines outlined in section 7. The lithospheric model IRPI used in the following computations is given in Table V.

In order to obtain a gross agreement of both the waveforms and relative amplitudes at different stations, it was found that a 17.5 km deep source located at A (see Fig. 18) with a rake of 230° on a fault dipping 70° toward the NE had to be assumed. A source duration of 0.6 s reproduces quite well the frequency content of most of the signal, provided the shock is repeated after 0.3 s. To model the longer duration of the observed recordings, more point sources have to be added some seconds later. A clear example of the need of another point source is represented by the large acceleration peak in the Sturno recordings arriving at about 11 s (Fig. 16). This peak can be modeled by assuming a point source with the same focal mechanism but located at B (see Fig. 18) with origin time shifted by 9.4 s.

TABLE V

Thickness (km)	Density (g/cm^3)	P-wave velocity (km/s)	S-wave velocity (km/s)	Q_β
0.05	2.3	1.55	0.90	20
0.20	2.3	1.90	1.10	20
0.25	2.3	2.25	1.30	30
0.25	2.3	2.60	1.50	30
0.25	2.3	2.77	1.60	50
1.00	2.3	3.00	1.70	100
8.00	2.8	5.60	3.20	400
5.00	2.8	5.70	3.30	400
5.00	2.8	4.80	3.10	400
17.00	2.9	6.80	3.90	400
47.50	3.4	8.10	4.65	400

Structure IRPI used in the Irpinia earthquake modeling.
It has been assumed that $Q_\alpha = 2.5\ Q_\beta$.

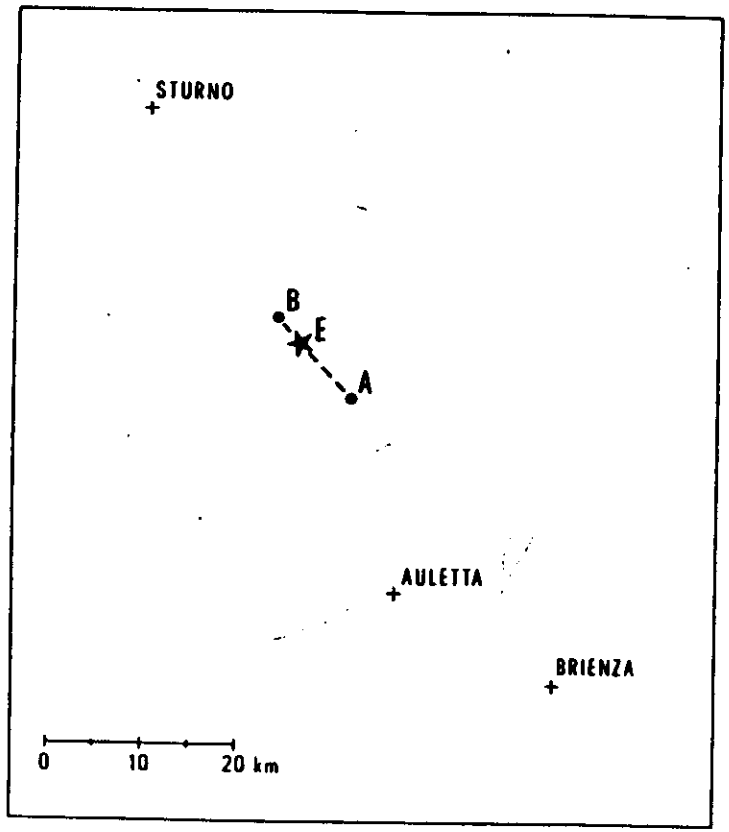

Fig. 18 Map showing the positions of the epicenter, E (40°46'N 15°18'E), the point sources, A and B, used in the construction of the synthetic signals shown in Fig. 19 and of the considered strong motion stations. Stations coordinates are:
Auletta (40°33'37"N 15°33'30"E)
Brienza (40°28'27"N 15°38'06"E)
Sturno (41°01'21"N 15°07'02"E).

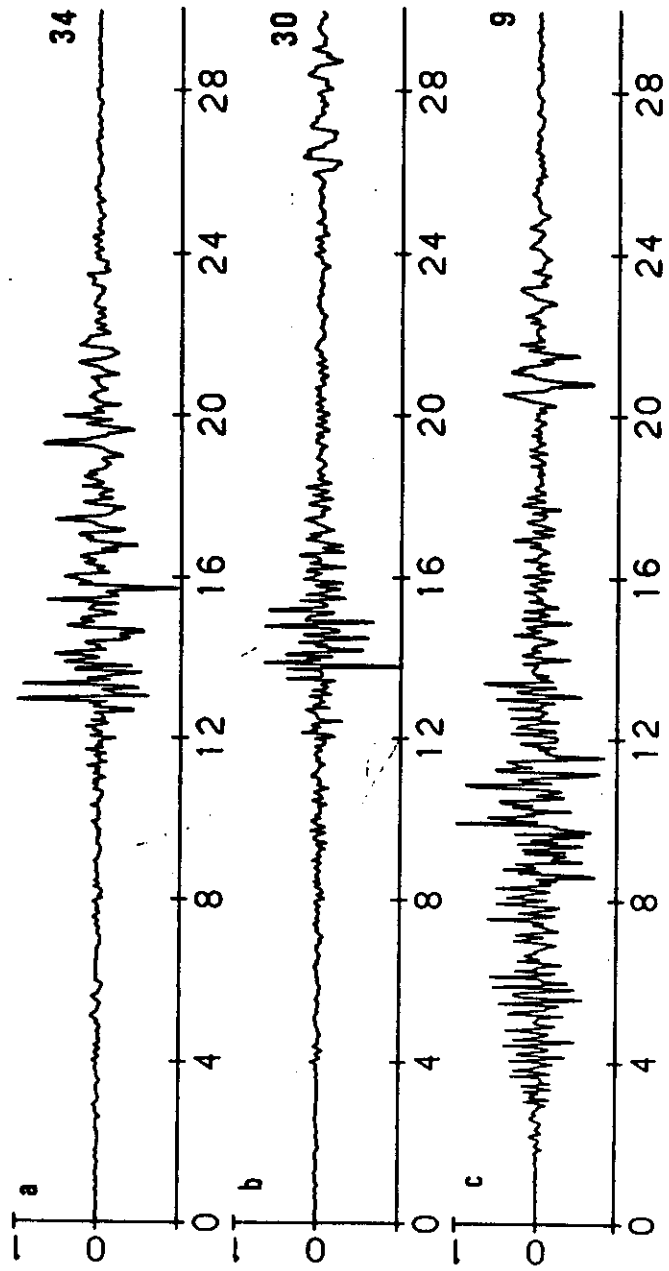

Fig. 19 Synthetic accelerations: a) Sturno, b) Brienza, c) Auletta stations. The peak acceleration is in units of 10^{-25} cm/s^2.

The synthetic accelerograms obtained in such a way are presented in Fig. 19 for the three stations Sturno, Brienza and Auletta. The amplitudes and the overall appearance of these signals matches quite well the observed ones and allow to estimate the seismic moment of the first two sources to be about 3×10^{25} dyne-cm, while the moment of the third one turns out to be about 5×10^{25} dyne-cm. Of course, a close waveform matching is still out of our reach, until a better understanding of the high frequency behavior of earthquake rupturing will be achieved and until our theoretical modeling will be extended to two- and three-dimensional laterally heterogeneous structures.

References

Aki, K. and Richards, P.G. (1980). "Quantitative Seismology". Freeman and Co., San Francisco.

Alekseev, A.S. and Mikhailenko, B.G. (1980). **J. Geophys.**, 48, 161-172.

Allen, C.R. and Nordquist, J.M. (1972). **U. S. Geol. Surv. Profess. Paper**, 787, 16-23.

Bath, M. (1974). "Spectral Analysis in Geophysics". Elsevier Scientific Publishing Co., Amsterdam.

Ben-Menahem, A. (1961). **Bull. Seism. Soc. Am.**, 51, 401-435.

Ben-Menahem, A. and Harkrider, D.G. (1964). **J. Geophys.**, 69, 2605-2620.

Ben-Menahem, A. and Singh, S.J. (1981). "Seismic Waves and Sources". Springer, New York.

Ben-Menahem, A. and Vered, M. (1973). **Bull. Seism. Soc. Am.**, 63, 1611-1636.

Berardi, R., Berenzi, A. and Capozza, F. (1981). **Tech. Rept. CNEN-ENEL**, Rome, Italy.

Biehler, S., Kovach, R.L. and Allen, C.R. (1964). In "Marine Geology of Gulf of California" (T. Van Andel and G. Shor, eds.), 126-196. Am. Assoc. Petrol. Geologists Mem. 3.

Biswas, N.N. and Knopoff, L. (1974). **Geophys. J. R. astr. Soc.**, 36, 515-539.

Boatwright, J. (1982). **Bull. Seism. Soc. Am.**, 72, 1049-1068.

Boore, D.M. and Joyner, W.B. (1978). **Bull. Seism. Soc. Am.**, 68, 283-300.

Bouchon, M. (1981). **Bull. Seism. Soc. Am.**, 71, 959-971.

Brune, J.N. (1962). **Bull. Seism. Soc. Am.**, 52, 109-112.

Burdick, L.J. and Mellman, G.R. (1976). **Bull. Seism. Soc. Am.**, 66, 1485-1499.

Burridge, R. and Knopoff, L. (1964). **Bull. Seism. Soc. Am.**, 54, 1875-1888.

Campillo, M., Bouchon, M. and Massinon, B. (1984). **Bull. Seism. Soc. Am.**, 74, 79-90.

Chapman, C.H. (1978). **Geophys. J. R. astr. Soc.**, 54, 481-518.

Chiaruttini, C., Costa, G. and Panza, G.F. (1985). **J. Geophys.**, 58, 189-196.

Christensen, R.M. (1982). "Theory of Viscoelasticity - an Introduction" (Second ed.), Academic Press, New York.

Cormier, V.F. (1980). **Bull. Seism. Soc. Am.**, 70, 691-716.

Cormier, V.F. and Richards, P.G. (1977). **J. Geophys.**, 43, 3-31.

Del Pezzo, E., Iannaccone, G., Martini, M. and Scarpa, R. (1983). **Bull. Seism. Soc. Am.**, 73, 187-200.

Deschamps, A. and King, G.C.P. (1983). **Earth Plan. Sci. Lett.**, 62, 296-304.

Ebel, J.E. and Helmberger, D.V. (1982). **Bull. Seism. Soc. Am.**, 72, 413-437.

Fuchs, K. (1969). **J. Phys. Earth**, 16, Special Issue, 27-41.

Fuchs, K. and Müller, G. (1971). **Geophys. J. R. astr. Soc.**, 23, 417-433.

Futtermann, W.I. (1962). **J. Geophys. Res.**, 67, 5279-5291.

Ha, J. (1984). **Geophys. J. R. astr. Soc.**, 79, 863-873.

Harkrider, D.G. (1964). **Bull. Seism. Soc. Am.**, 54, 627-679.

Harkrider, D.G. (1970). **Bull. Seism. Soc. Am.**, 60, 1937-1987.

Hartzell, S.H. (1978). **Geophys. Res. Lett.**, 5, 1-4.

Harvey, D.J. (1981). **Geophys. J. R. astr. Soc.**, 66, 37-69.

Haskell, N.A. (1953). **Bull. Seism. Soc. Am.**, 43, 17-34.

Heaton, T.H. and Helmberger, D.V. (1977). **Bull. Seism. Soc. Am.**, 67, 315-330.

Helmberger, D.V. (1968). **Bull. Seism. Soc. Am.**, 58, 179-214.

Ingate, S.F., Bock, G. and King, R. (1983). **Geophys. J. R. astr. Soc.**, 75, 261-274.

Kanamori, H. (1979). **Bull. Seism. Soc. Am.**, 69, 1645-1670.

Kennett, B.L.N. (1983). "Seismic Wave Propagation in Stratified Media". Cambridge University Press, Cambridge.

Kind, R. (1978). **J. Geophys.**, 44, 603-612.

Knopoff, L. (1964a). **Bull. Seism. Soc. Am.**, 54, 431-438.

Knopoff, L. (1964b). **Rev. Geophys.**, 2, 625-660.

Knopoff, L., Aki, K., Archambeau, C.B., Ben-Menahem, A. and Hudson, J.A. (1964). **J. Geophys. Res.**, 69, 1655-1657.

Korn, M. and Müller, G. (1983). **Geophys. J. R. astr. Soc.**, 72, 541-556.

Koyama, J. (1985). **Tectonophysics**, 118, 227-242.

Minster, J.B. (1980). **Proceedings of the Enrico Fermi International School of Physics** (A. Dziewonski and E. Boschi, eds.), 152-212. Amsterdam, North Holland.

Müller, G. (1969). **Z. Geophys.**, 35, 347-371.

Müller, G. (1983). **J. Geophys.**, 54, 20-29.

O'Connell, R.J. and Budiansky, B. (1978). **Geophys. Res. Lett.**, 5, 5-8.

Olson, A.H., Orcutt, J.A. and Frazier, G.A. (1984). **Geophys. J. R. astr. Soc.**, 77, 421-460.

Panza, G.F. (1985). **J. Geophys.**, 58, 125-145.

Panza, G.F., Schwab, F. and Knopoff, L. (1972). **Geophys. J. R. astr. Soc.**, 30, 273-280.

Panza, G.F., Schwab, F. and Knopoff, L. (1973). **Geophys. J. R. astr. Soc.**, 34, 265-278.

Panza, G.F. and Suhadolc, P. (1986). **In** "..." Complete strong motion synthetics (B.A. Bolt, ed.) Academic Press. **In press.**

Panza, G.F., Suhadolc, P. and Chiaruttini, C. (1986). Exploitation of broadband networks through broadband synthetic seismograms. **Annales Geophysicae. In press.**

Pekeris, C.L. (1948). **Geol. Soc. Am. Mem.** 27, 1-116.

Pilant, W.L. (1979). "Elastic Waves in the Earth". Elsevier, Amsterdam.

Schwab, F. (1970). **Bull. Seism. Soc. Am.**, 60, 1491-1520.

Schwab, F., Cuscito, M., Panza, G.F. and Nakanishi, K. (1986). Surface-wave computations and the synthesis of theoretical seismograms at high frequency. II. Group velocity, attenuation due to anelasticity and frequency intervals. **In preparation.**

Schwab, F. and Knopoff, L. (1971). **Bull. Seism. Soc. Am.**, 61, 893-912.

Schwab, F. and Knopoff, L. (1972). **In** "Methods in Computational Physics" (B.A. Bolt, ed.), 11, 87-180. Academic Press.

Schwab, F. and Knopoff, L. (1973). **Bull. Seism. Soc. Am.**, 63, 1107-1117.

Schwab, F., Nakanishi, K., Cuscito, M., Panza, G.F., Liang, G. and Frez, J. (1984). **Bull. Seism. Soc. Am.**, 74, 1555-1578.

Spudich, P. and Ascher, U. (1983). **Geophys. J. R. astr. Soc.**, 75, 101-124.

Suhadolc, P. and Panza, G.F. (1985). **J. Geophys.**, 58, 183-188.

Swanger, H.J. and Boore, D.M. (1978). **Bull. Seism. Soc. Am.**, 68, 907-922.

Tolstoy, I. (1956). **J. Acoust. Soc. Am.**, 28, 1182-1192.

Wang, C.Y. and Herrmann, R.B. (1980). **Bull. Seism. Soc. Am.**, 70, 1015-1036.

earthquake and corresponding to the observed ones of Fig. 1. The zero-to-peak acceleration for a 1 dyne·cm seismic moment is shown in units of cm/s^2 on the left side of each trace. See the text for details.

Fig. 5 Amplitude spectra of the observed (top) and synthetic (bottom) accelerograms relative to the Sturno station. The maximum amplitudes are normalized to one.

Fig. 6 Rupturing process of the Irpinia 1980 earthquake used to model the synthetics of Fig. 4. See the text for details.

Fig. 7 Epicenter (indicated by a star) location of the Friuli, September 11, 1976 M=5.6 aftershock.

Fig. 8 Accelerogram relative to the Friuli, September 11, 1976 M=5.6 aftershock recorded at the station Buia (top). The peak ground acceleration (normalized to one in the Figure) is 91 cm/s^2. The same accelerogram gaussian filtered at 10 Hz (middle). The amplitude spectra corresponding to the middle trace (bottom).

Fig. 9 a) Distribution versus depth of elastic and anelastic properties for the Friuli structural model used in the synthetic accelerogram computation.
b) Distribution versus depth of elastic and

anelastic properties for the upper two kilometers of the Friuli structural model.

Fig. 10 The synthetic accelerogram (one point source) corresponding to the observed trace of Fig. 8 is shown above, the zero-to-peak amplitude (for a 1 dyne·cm seismic moment) being 5.5×10^{-22} cm/s^2. Its amplitude spectra is shown below.

Fig. 11 The synthetic accelerogram (sum of three point sources) corresponding to the observed trace of Fig. 8 is shown above, the zero-to-peak amplitude (for a 1 dyne·cm seismic moment) being 5.8×10^{-22} cm/s^2. Its amplitude spectra is shown below.

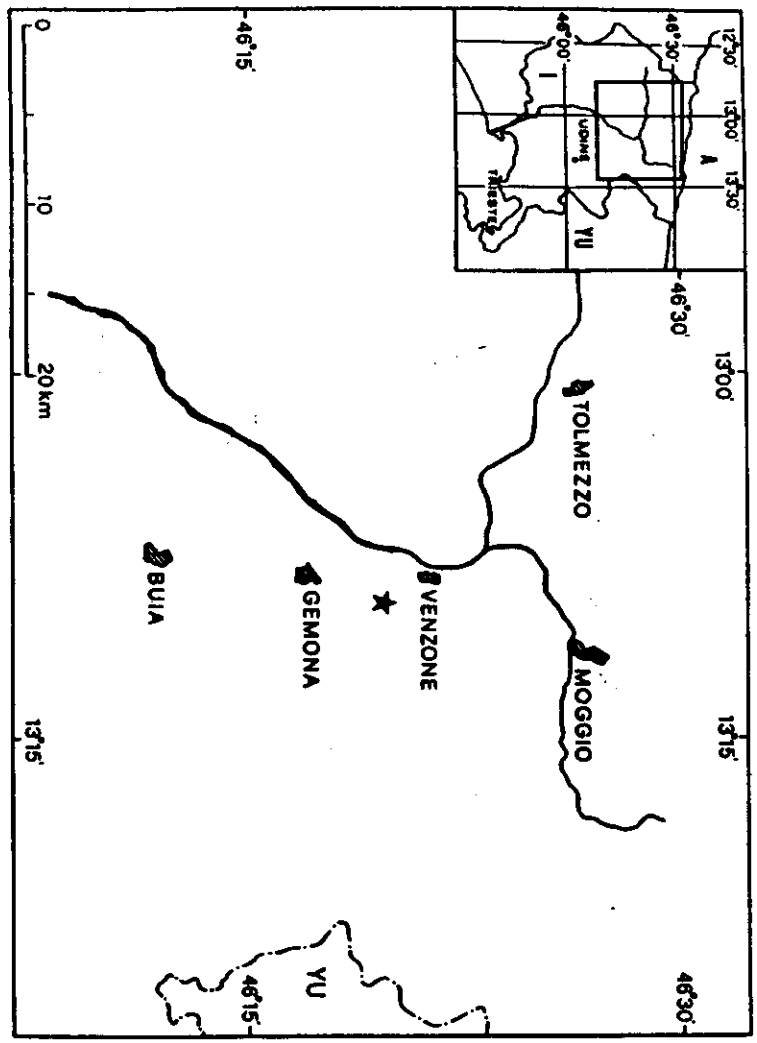

Fig. 7

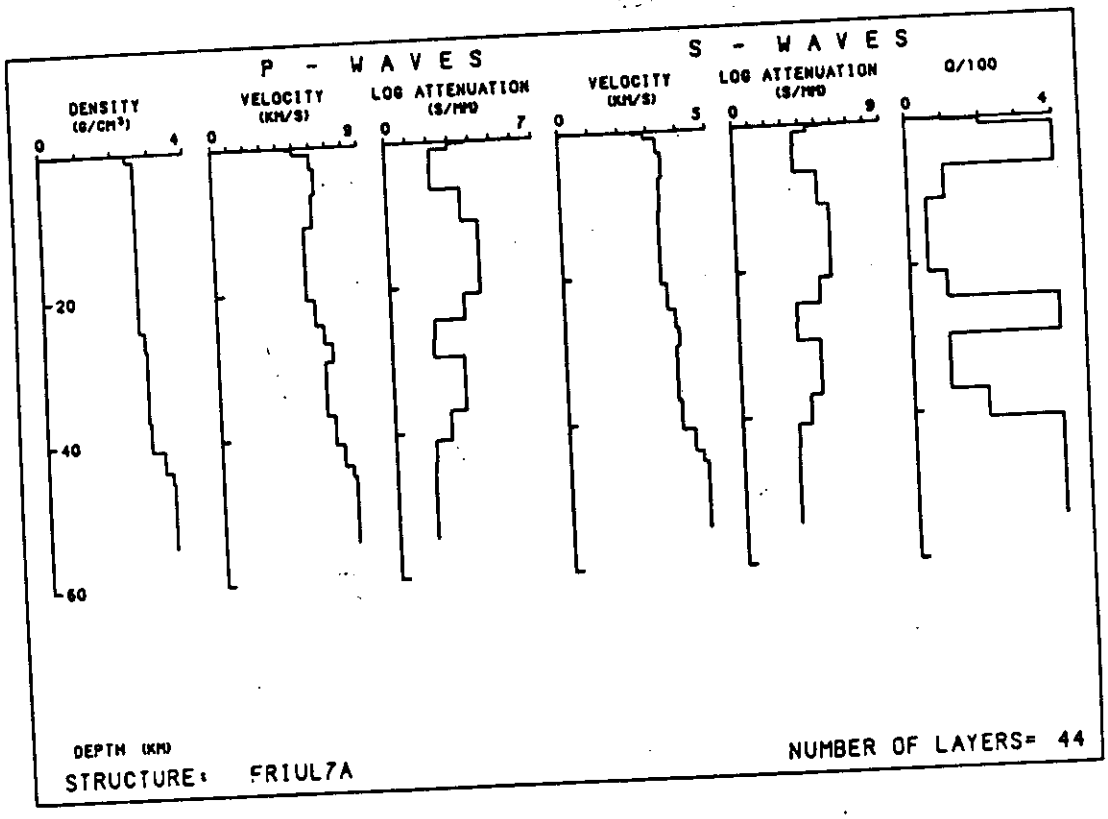
P - WAVES
S - WAVES
DENSITY (G/CM³)
VELOCITY (KM/S)
LOG ATTENUATION (S/MPD)
VELOCITY (KM/S)
LOG ATTENUATION (S/MPD)
Q/100
0
4
0
9
0
7
0
5
0
9
0
4
20
40
60
DEPTH (KM)
STRUCTURE: FRIUL7A
NUMBER OF LAYERS= 44

FIG. 9a

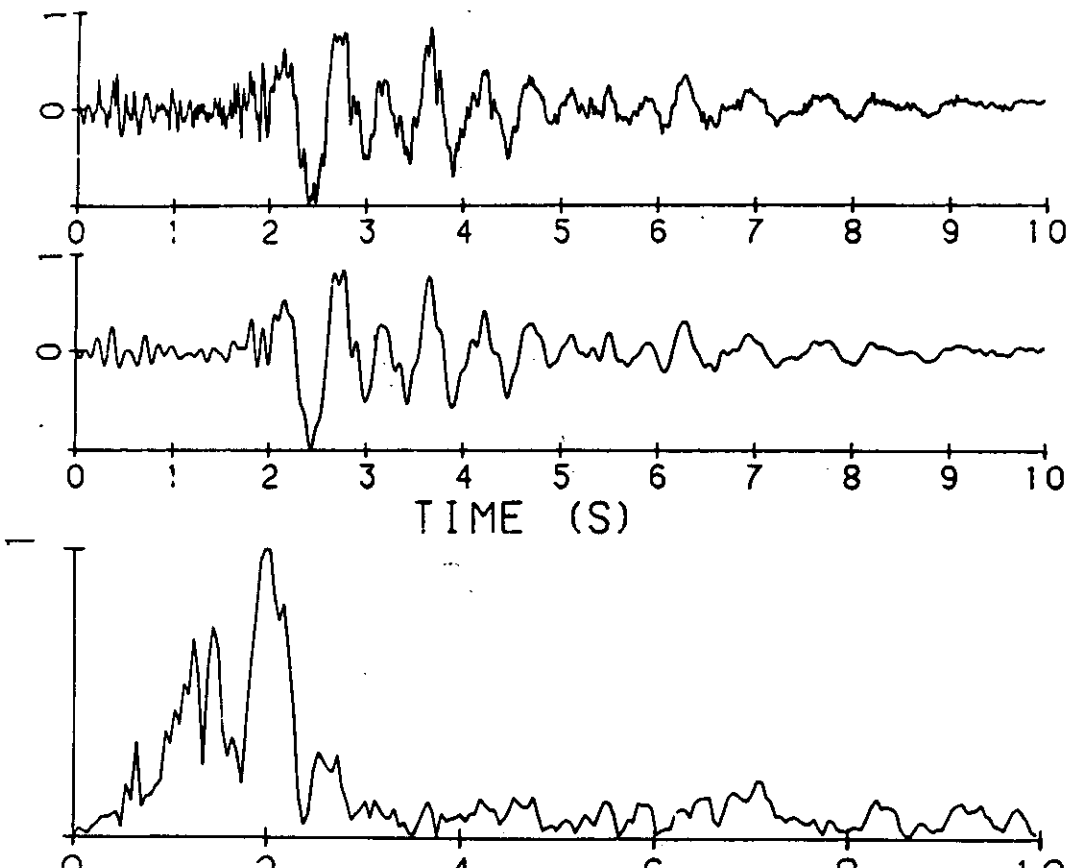
0
0 1 2 3 4 5 6 7 8 9 10
0
0 1 2 3 4 5 6 7 8 9 10
TIME (S)
0 2 4 6 8 10
FREQUENCY (HZ)

FIG. 8.

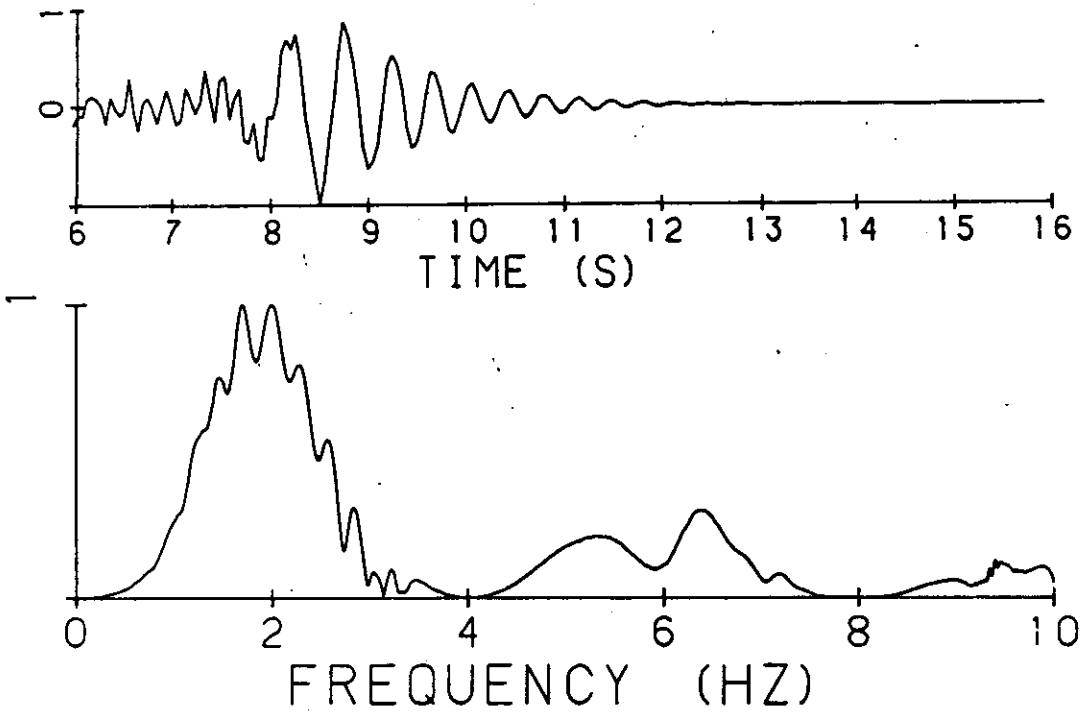
0
6 7 8 9 10 11 12 13 14 15 16
TIME (S)
0 2 4 6 8 10
FREQUENCY (HZ)

FIG. 10

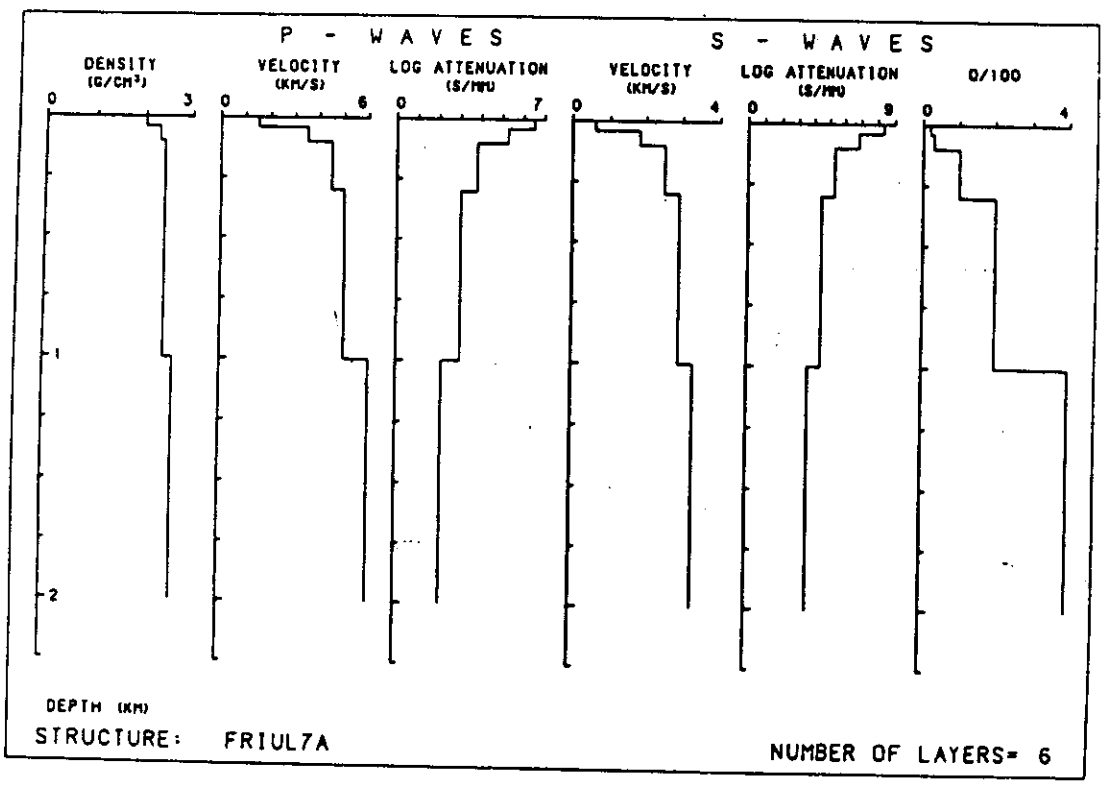
P - WAVES
S - WAVES
DENSITY (G/CM³)
VELOCITY (KM/S)
LOG ATTENUATION (S/MU)
VELOCITY (KM/S)
LOG ATTENUATION (S/MU)
Q/100
0 3
0 6
0 7
0 4
0 9
0 4
1
2
DEPTH (KM)
STRUCTURE: FRIUL7A
NUMBER OF LAYERS= 6

FIG. 9b

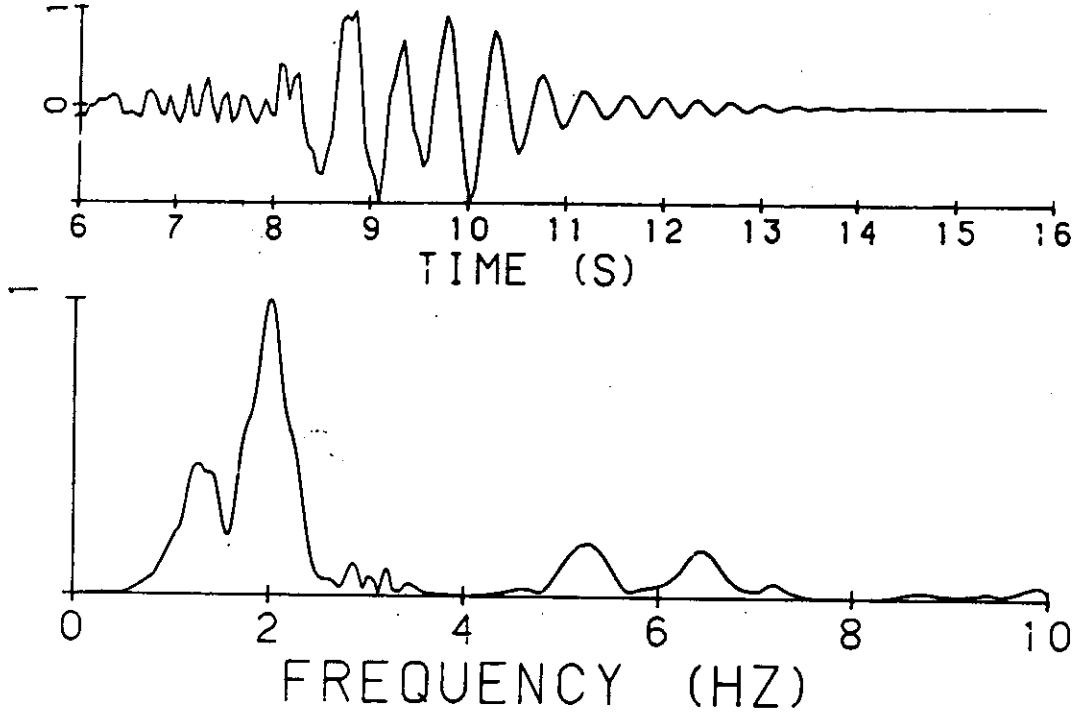

FIG. 11